Chapter V. Results

V.1. THERMODYNAMIC STUDIES OF PHOSPHOLIPID MONOLAYERS

V.1.1. Studies at a controlled temperature of 24 ºC

To simplify the system monolayers were studied as model membranes at a room temperature of 24 ºC. All isotherms were obtained as described in the Experimental Methods chapter.

V.1.1.1. POPE and POPC mixtures

Figure 47 shows the variation of the surface pressure as a function of the molecular area for monolayers of pure POPE and POPC and binary mixtures of both phospholipids.

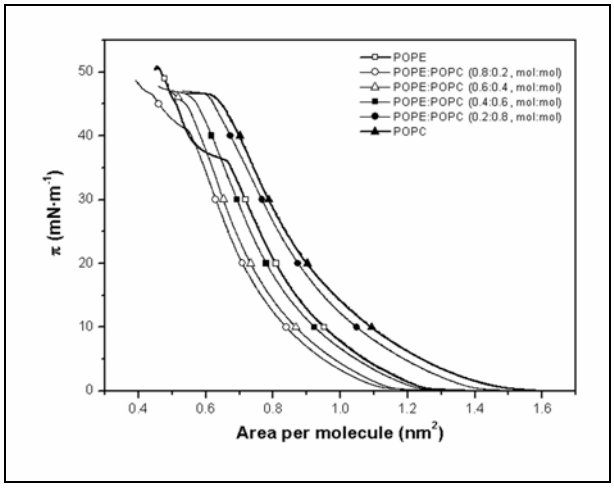

Figure 47. Isotherms of pure POPE, pure POPC and mixed POPE:POPC monolayers at 24 ºC.

The monolayer of pure POPE exhibits the transition namely LC-LC' at a surface pressure of 36.0 $mN \cdot m^{-1}$. Interestingly, another transition in the POPE isotherm can be observed at a surface pressure of 45.5 $mN \cdot m^{-1}$ and above this value the monolayer collapses at a surface pressure of 50.7 $mN \cdot m^{-1}$. The monolayer of pure POPC is always

in the LE phase and shows a collapse surface pressure of 46 $mN \cdot m^{-1}$. The phase transition of POPE gradually disappears when POPC is incorporated into the monolayer and disappears for a mixture value of $\chi_{POPC} = 0.6$. The surface pressure at which the LC-LC' transition is observed is modified in the presence of POPC as a result of the miscibility between POPE and POPC molecules. Monolayers with values of $\chi_{POPC} \leq 0.6$ present smaller molecular areas than pure POPE below the first transition, indicating that the POPC molecules can occupy the space between POPE molecules, thus decreasing the area per molecule of the mixture.

Collapse pressures of mixed monolayers do not show a linear relationship with collapse surface pressures of pure components. Collapse surface pressures for mixed monolayers with values of $\chi_{POPC} \geq 0.6$ are governed by the pure POPC collapse surface pressure.

Values of excess area, calculated according to equation V, are shown in Figure 48 as a function of composition and at various surface pressures. A minimum value is found at a surface pressure of 5 $mN \cdot m^{-1}$ and a molar fraction of $\chi_{POPC} = 0.2$. The negative values found in most of the compositions and at most of the surface pressures studied suggest that the predominant forces in the interaction between the molecules are attractive forces.

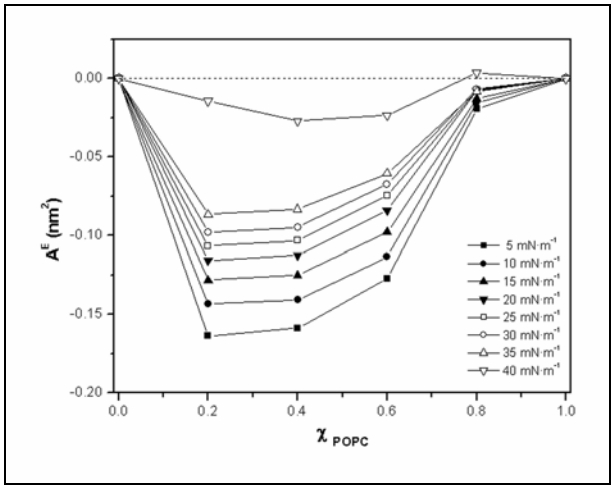

Figure 48. Excess area per molecule as a function of composition for pure and mixed POPE:POPC monolayers.

A^E values (Figure 48) decrease as the surface pressure increases and reach zero for the unique surface pressure of 40 $mN \cdot m^{-1}$. When surface pressure increases, the phospholipid molecules are forced closer together and steric repulsion arises. This steric effect causes the decrease in the absolute values of A^E.

Figure 49 shows variations of $\Delta_{mix}G$ in mixed POPE:POPC monolayers as a function of the molar fraction of POPC for different surface pressures. All values of $\Delta_{mix}G$ are negative for the entire range of surface pressures studied (5-40 $mN \cdot m^{-1}$) with a minimum value of $\chi_{POPC} = 0.4$. Negative values of $\Delta_{mix}G$ imply that the monolayer is stable at this POPC molar fraction and surface pressure. This suggests that POPE and POPC develop attractive intermolecular forces with maximum stability at a value of $\chi_{POPC} = 0.4$. Interestingly, very high absolute values of $\Delta_{mix}G$ can be found at higher surface pressures. This can be explained by the shorter intermolecular distances associated with high surface pressures.

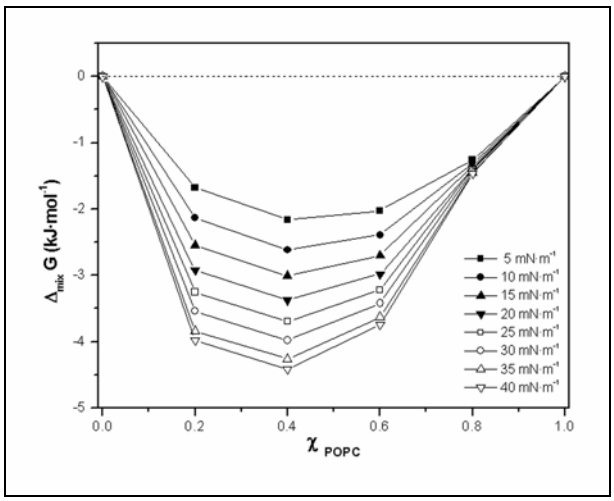

Figure 49. Variation of the Gibbs energy of mixing with the molar fraction of POPC at different surface pressures.

V.1.1.2. POPC and CL mixtures

Figure 50 shows the variation of the surface pressure as a function of the molecular area for monolayers of pure POPC, pure CL and mixtures of both phospholipids.

All monolayers presented in Figure 50 are in the LE phase and no phase transitions are observed at this temperature. The area per molecule of the mixed monolayers increases when CL is progressively incorporated into the monolayer. The collapse surface pressures of mixed monolayers decrease linearly within the values of pure components: 46.0 $mN \cdot m^{-1}$ and 43.1 $mN \cdot m^{-1}$ for POPC and CL respectively. This linearity of the collapse surface pressures shows that the molecules are completely miscible.

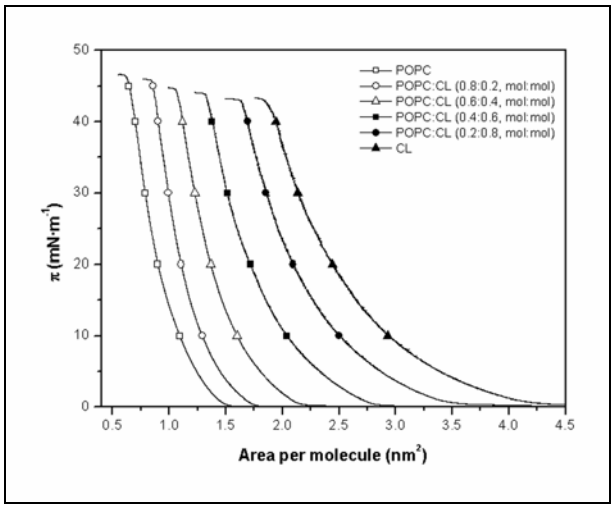

Figure 50. Isotherms of pure POPC, pure CL and mixed POPC:CL monolayers at 24 ºC.

Values of excess area, calculated according to equation V, are shown in Figure 51 as a function of composition at various surface pressures.

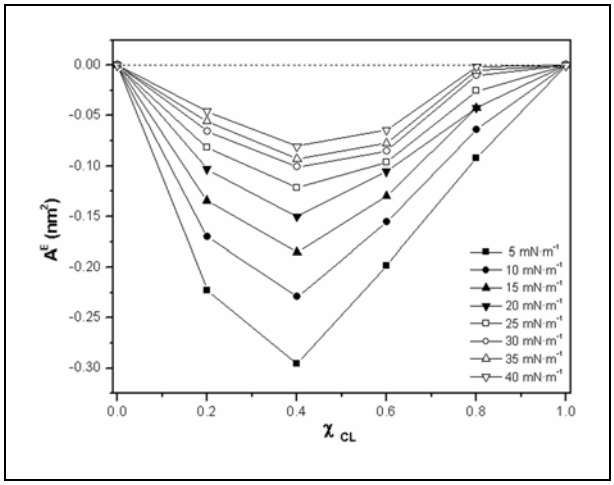

Figure 51. Excess area per molecule as a function of composition for pure and mixed POPC:CL monolayers.

From Figure 51 it can be seen that all A^E values are negative for all compositions and surface pressures analyzed, which suggests that attractive intermolecular forces between POPC and CL molecules predominate in these monolayers. A minimum A^E value is found at $\chi_{CL} = 0.4$ for all surface pressures analyzed. When the CL molar fraction is increased repulsive forces arise between the negatively charged CL molecules and counteract the attractive intermolecular forces, thus decreasing the absolute values of A^E. At a value of $\chi_{CL} = 0.8$ and surface pressures greater than 25 $mN \cdot m^{-1}$, attractive and repulsive forces are balanced and A^E values tend to zero.

Figure 52 shows the variations of $\Delta_{mix}G$ of mixed POPC:CL monolayers as a function of the molar fraction of CL at different surface pressures. All values of $\Delta_{mix}G$ are negative for the entire range of surface pressures studied (5-40 $mN \cdot m^{-1}$) with a minimum value when $\chi_{CL} = 0.4$. Negative values of $\Delta_{mix}G$ show that monolayers are stable for the range of surface pressures and CL molar fraction studied, which suggests the presence of attractive intermolecular forces between POPC and CL molecules. Maximum monolayer stability is found when $\chi_{CL} = 0.4$ at all surface pressures studied. Interestingly, lower absolute values of $\Delta_{mix}G$ are observed at higher surface pressures. As in the case of A^E values, the increase in surface pressure produces a decrease in the absolute values of $\Delta_{mix}G$ due to the proximity of CL molecules.

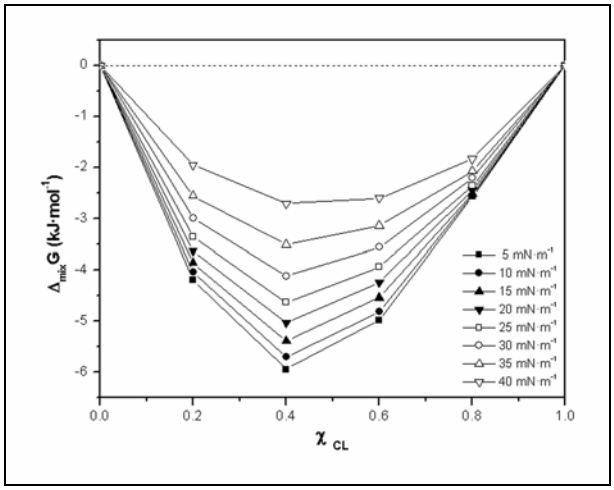

Figure 52. Variation of the Gibbs energy of mixing with the molar fraction of CL at different surface pressures.

V.1.1.3. POPE and CL mixtures

Figure 53 shows the variation of the surface pressure as a function of the molecular area for pure POPE, pure CL and mixtures of both phospholipids.

Pure POPE and CL monolayers are described in sections V.1.1.1. and V.1.1.2, respectively. Mixed monolayers are always in the LE phase and do not exhibit any transition at this temperature. When CL is progressively incorporated into the monolayer the area per molecule of the mixed monolayer increases. If the pure POPE isotherm is not considered, the collapse surface pressure of monolayers decreases monotonically as the CL molar fraction increases. This suggests a certain level of miscibility between POPE and CL molecules at this temperature and within the range $\chi_{CL} = 0.2\text{-}1.0$.

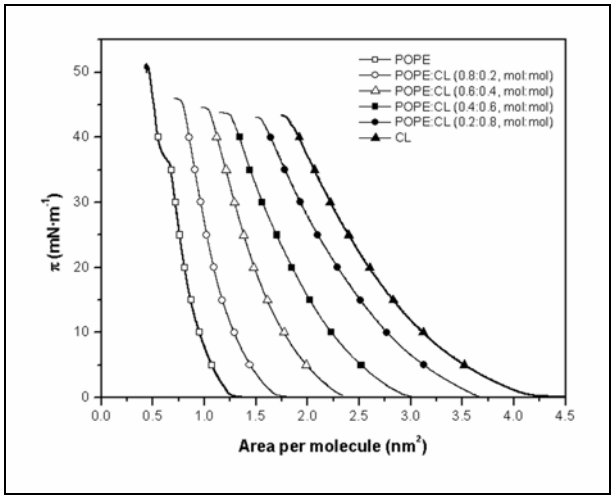

Figure 53. Isotherms of pure POPE, pure CL and mixed POPE:CL monolayers at 24 ºC.

Values of excess area, calculated using equation V, are shown in Figure 54 as a function of composition at various surface pressures.

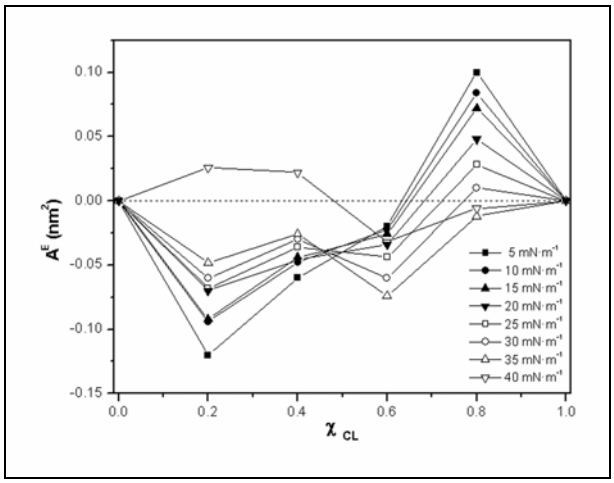

Figure 54. Excess area per molecule as a function of composition for pure and mixed POPE:CL monolayers.

Values of A^E are positive at a high molar fraction of CL, $\chi_{CL} \geq 0.8$, and decrease as surface pressure increases, while at a low molar fraction of CL the values of A^E are negative. Positive A^E values are indicative of instability in the monolayer due to the appearance of repulsive intermolecular forces between the molecules. A minimum value of A^E exists when $\chi_{CL} = 0.2$ at almost all surface pressures analyzed and the absolute value of A^E decreases as surface pressure increases. At the unique surface pressure of 40 mN·m^{-1} the values of A^E are randomly distributed close to the zero value that represents ideal behaviour. This can be explained in two ways: either that at a surface pressure of 40 mN·m^{-1}, molecules in the monolayer are ideally mixed or that at this surface pressure the two phospholipids are completely segregated from each other and form domains.

Figure 55 shows the variation of $\Delta_{mix}G$ of mixed POPE:CL monolayers as a function of the molar fraction of CL at different surface pressures. A minimum in the plot at a value of $\chi_{CL} = 0.2$ exists at almost all surface pressures. The minimum in the plot indicates the more stable mixed monolayer assayed. At a high molar fraction of CL, $\chi_{CL} \geq 0.8$, values of $\Delta_{mix}G$ tend to positive values. Similarly to the A^E analysis, monolayers with a high molar fraction of CL present repulsion between neighbouring molecules, as can be seen from the decrease in the absolute values of $\Delta_{mix}G$.

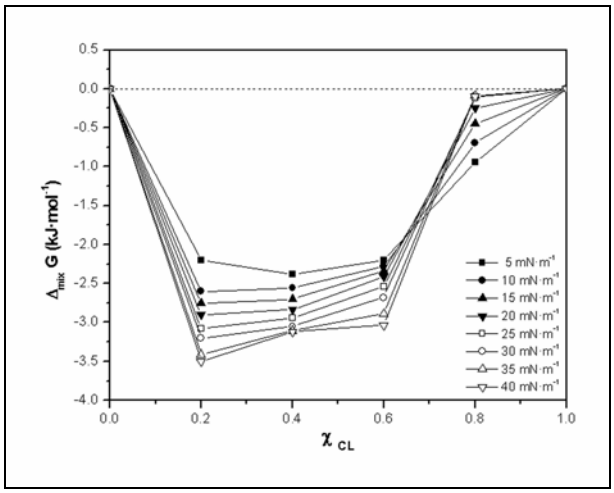

Figure 55. Variation of the Gibbs energy of mixing with the molar fraction of CL at different surface pressures.

Interestingly, when $\chi_{CL} < 0.8$ higher absolute values of $\Delta_{mix}G$ are observed as surface pressures increases whereas when $\chi_{CL} \geq 0.8$ the absolute values of $\Delta_{mix}G$ decrease in response to increasing surface pressure. This suggests that CL molecules, at CL molar fractions lower than 0.8, can be compacted without repulsion and that the predominant intermolecular forces in the monolayer are attractive forces. For values of χ_{CL} between 0.8 and 1.0, the lateral compaction of molecules creates intermolecular repulsion forces between phospholipids in the monolayer.

The miscibility of POPE and CL was studied in depth to try and account for the sudden LC-LC' transition disappearance in the first mixed monolayer. Monolayers with values of $\chi_{CL} = 0.05$ and $\chi_{CL} = 0.10$ were assayed (Figure 56). On the one hand, the behaviour of the monolayer with $\chi_{CL} = 0.10$ is completely consistent with that of the other mixed monolayers presented in Figure 53 when CL is progressively introduced into the mixture. On the other hand, the monolayer with $\chi_{CL} = 0.05$ displays several differences: firstly, this monolayer has two collapse surface pressures, one at a surface pressure of ~ 45.9 mN·m^{-1} and another at a surface pressure of ~ 50.2 mN·m^{-1}; secondly, the LC-LC' transition in this monolayer occurs at a surface pressure of ~ 39.1 mN·m^{-1}, which suggests a certain level of miscibility between POPE and CL molecules at this CL molar fraction.

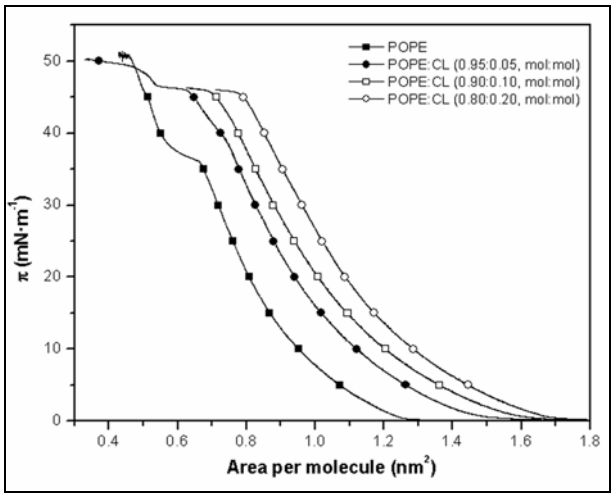

Figure 56. More accurate analysis of POPE and CL mixed monolayers for $\chi_{CL} \leq 0.20$.

V.1.2. Studies at a controlled temperature of 37 ºC

Once the thermodynamic analysis had been performed at a temperature of 24 ºC, the process was repeated at 37 ºC since many cells and bacteria live at this temperature. All isotherms were performed as described in the Experimental Methods section.

V.1.2.1. POPE and POPC mixtures

Figure 57 shows the variation of the surface pressure as a function of the molecular area for pure POPE, pure POPC and mixtures of both phospholipids.

All monolayers shown in Figure 57 are in the LE phase and no phase transitions can be detected at this temperature. Pure POPE presents a lower area per molecule than pure POPC, while mixed monolayers show intermediate values between the two pure phospholipids. The collapse surface pressures of mixed monolayers show a linear relationship between the collapse surface pressures of the respective components, which indicates the miscibility between POPE and POPC molecules.

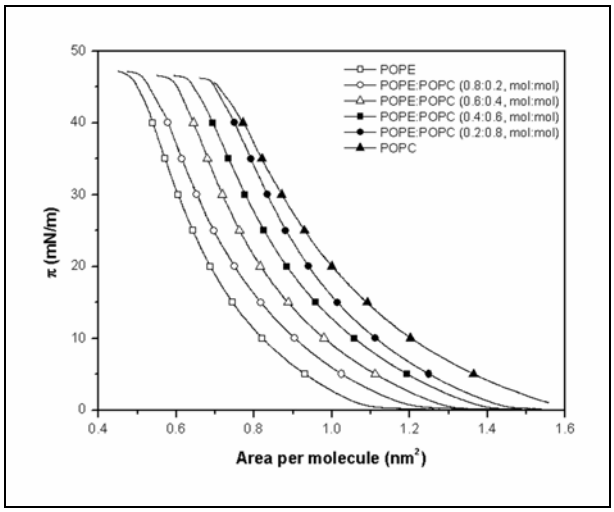

Figure 57. Isotherms of pure POPE, pure POPC and mixed POPE:POPC monolayers at 37 ºC.

Values of excess area, calculated with equation V, are shown in Figure 58 as a function of composition at various surface pressures. For compositions with values of $\chi_{POPC} \leq 0.6$, A^E values are close to the zero value that represents ideal behaviour, while for values of $\chi_{POPC} = 0.8$, a minimum ($\pi \leq 15$ mN·m^{-1}) and a maximum ($\pi \geq 30$ mN·m^{-1}) value of A^E exist. Values of A^E close to the zero point indicate that the molecules in the monolayer display ideal behaviour or total immiscibility. The existence of a minimum and a maximum in the plot, at the same POPC molar fraction ($\chi_{POPC} = 0.8$), indicates that POPC molecules exhibit different behaviour at different surface pressures. At low surface pressures ($\pi \leq 15$ mN·m^{-1}), attractive forces exist between POPC-POPC and/or POPE-POPC pairs, while at higher surface pressures ($\pi \geq 30$ mN·m^{-1}) the predominant forces between molecules are repulsive.

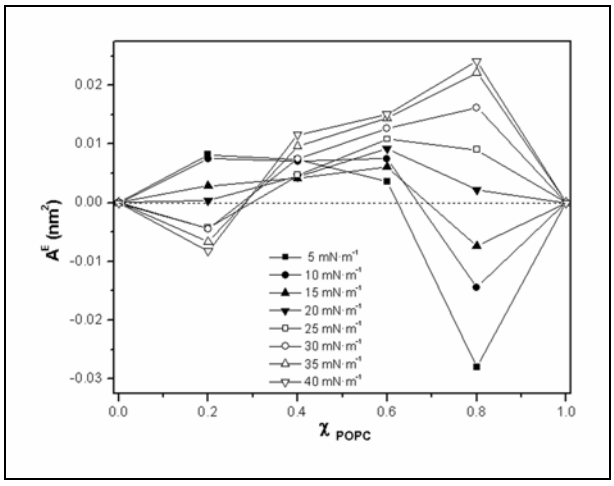

Figure 58. Excess area per molecule as a function of composition for pure and mixed POPE:POPC monolayers.

When $\chi_{POPC} \leq 0.2$, A^E values decrease as surface pressure is increased, whereas when $\chi_{POPC} > 0.2$, A^E values increase as surface pressure is increased.

Figure 59 shows the variation of $\Delta_{mix}G$ of mixed POPE:POPC monolayers as a function of the molar fraction of POPC at different surface pressures.

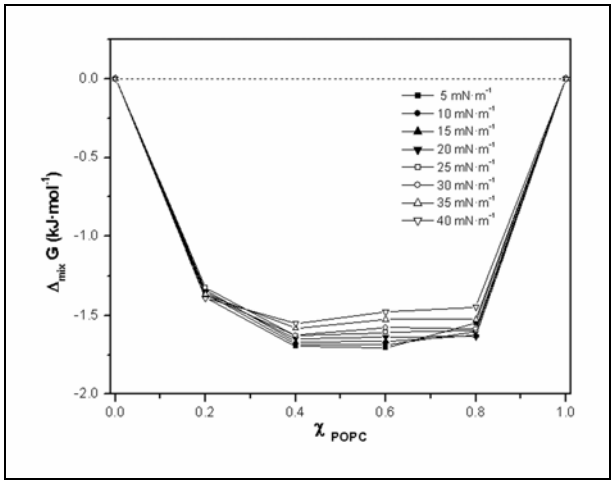

Figure 59. Variation of the Gibbs energy of mixing with the molar fraction of POPC at different surface pressures.

Values of $\Delta_{mix}G$ are all negative with a minimum range of χ_{POPC} = 0.4-0.8. At surface pressures below 30 mN·m^{-1}, values of $\Delta_{mix}G$ are very similar and the absolute value for higher surface pressures. Negative $\Delta_{mix}G$ values indicate monolayer stability and the decrease of $\Delta_{mix}G$ values as surface pressure increases can be attributed to a steric effect. Interestingly, $\Delta_{mix}G$ values are not dependent on the surface pressure at the value of χ_{POPC} = 0.2.

V.1.2.2. POPC and CL mixtures

Figure 60 shows the variation of surface pressure as a function of the molecular area for monolayers of pure POPC, pure CL and mixtures of both phospholipids.

All monolayers displayed in Figure 60 are in the LE phase since no phase transitions are observed at this temperature. The area per molecule of mixed monolayers increases

when CL is progressively incorporated into the monolayer and isotherms of mixed monolayers fall between the isotherms of the two pure phospholipids.

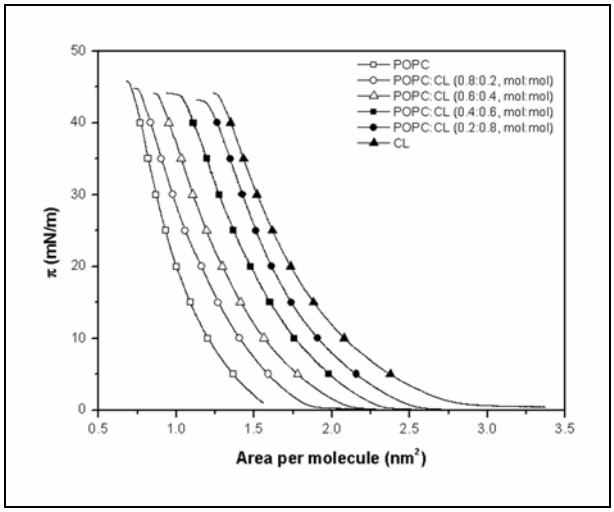

Figure 60. Isotherms of pure POPC, pure CL and mixed POPC:CL monolayers at 37 ºC.

Values of excess area, calculated using equation V, are shown in Figure 61 as a function of composition at various surface pressures.

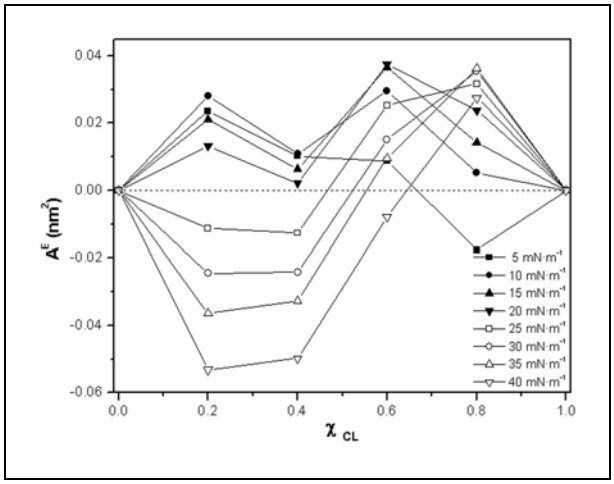

Figure 61. Excess area per molecule as a function of composition for pure and mixed POPC:CL monolayers.

It can be seen that almost all A^E values are positive at low surface pressures ($\pi \leq 20$ mN·m^{-1}) while negative A^E values appear at surface pressures greater than 25 mN·m^{-1} in the range $\chi_{CL} = 0.2\text{-}0.4$. Moreover, when $\chi_{CL} < 0.8$ the values of A^E decrease as surface pressure increases, whereas when $\chi_{CL} \geq 0.8$ the values of A^E display the opposite

behaviour. Positive A^E values at low surface pressures in the range χ_{CL} = 0.2-0.4 can be explained by the high mobility of hydrocarbon chains of both phospholipids at 37 ºC. At higher CL molar fractions, positive A^E values can be explained by the CL-CL repulsion due to the accumulation of negative surface charge in the monolayer. Negative A^E values at surface pressures greater than 25 $mN \cdot m^{-1}$ in the range χ_{CL} = 0.2-0.4 can be explained by the restriction of hydrocarbon chains to a smaller area, thus decreasing the interaction between them. At a higher CL molar fraction this effect cannot occur due to the repulsion between CL polar heads that prevents the compaction of the phospholipid molecules.

Figure 62 shows the variation of $\Delta_{mix}G$ of mixed POPC:CL monolayers as a function of the molar fraction of CL at different surface pressures.

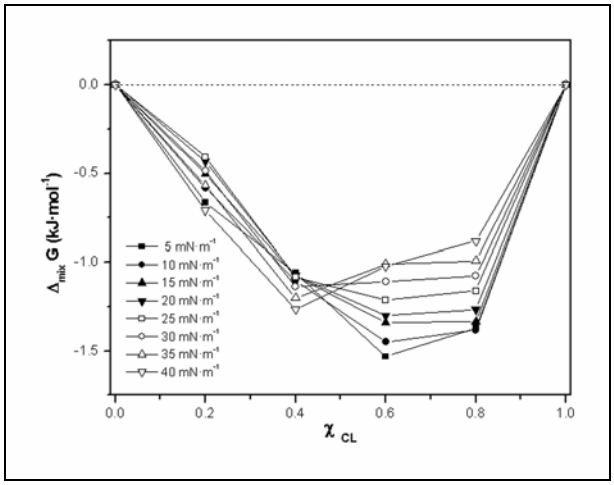

Figure 62. Variation of the Gibbs energy of mixing with the molar fraction of CL at different surface pressures.

All values of $\Delta_{mix}G$ are negative with a minimum at χ_{CL} = 0.6 for almost all surface pressures studied. When $\chi_{CL} \geq 0.6$, the absolute values of $\Delta_{mix}G$ decrease as surface pressure is increased, whereas when $\chi_{CL} < 0.6$, the $\Delta_{mix}G$ values are randomly distributed. As described in the previous sections, negative $\Delta_{mix}G$ values indicate stability in the monolayer and a minimum in the plot identifies the more stable monolayer of the POPC and CL mixture. When the CL molar fraction is increased, instability appears in the monolayer at high surface pressures. This instability can be explained by the proximity of CL molecules on the surface.

V.1.2.3. POPE and CL mixtures

Figure 63 shows the variation of surface pressure as a function of the molecular area for pure POPE, pure CL and mixtures of both phospholipids.

All monolayers shown in Figure 63 are always in the LE phase and exhibit no phase transition at this temperature. The area per molecule of mixed monolayers increases when CL is progressively incorporated into the monolayer. If pure POPE is not considered, the collapse surface pressure of mixed monolayers decreases monotonically as the CL molar fraction increases.

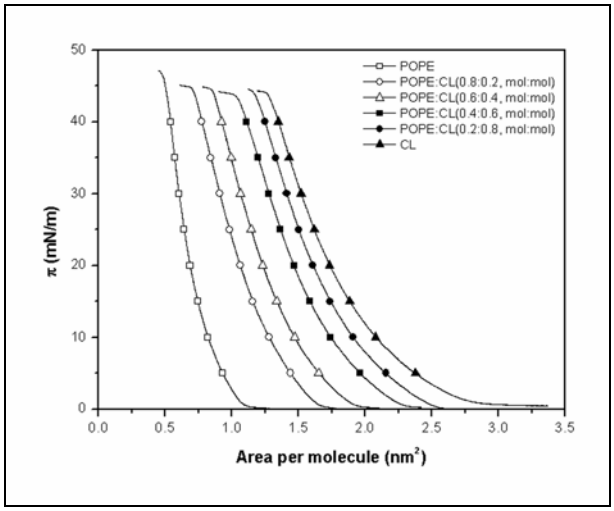

Figure 63. Isotherms of pure POPE, pure CL and mixed POPE:CL monolayers at 37 ºC.

Values of excess area, calculated using equation V, are shown in Figure 64 as a function of composition at various surface pressures.

All A^E values are positive in the entire range of surface pressures studied, with a maximum at $\chi_{CL} = 0.2$ but smoothed to a wider range at high surface pressures ($\pi \geq 35$ $mN \cdot m^{-1}$). A^E values decrease when surface pressure is increased in the monolayer for all molar fractions evaluated. Positive A^E values indicate instability in the monolayer due to repulsive forces between adjacent molecules. As with the A^E values of POPC and CL at 37 ºC, the absolute A^E values of POPE and CL decrease at high surface pressures due to the restriction of hydrocarbon chains to a smaller area.

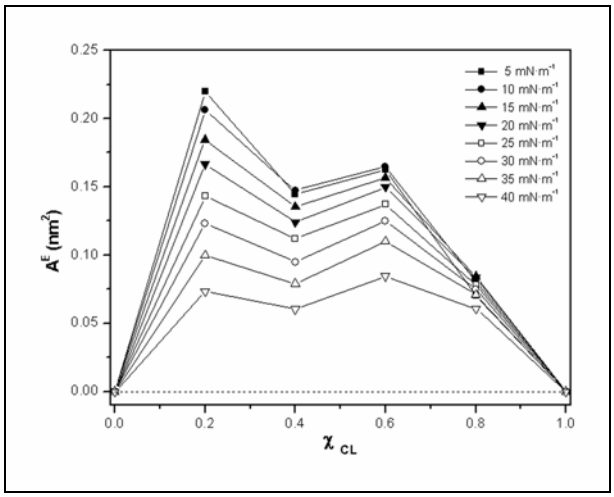

Figure 64. Excess area per molecule as a function of composition for pure and mixed POPE:CL monolayers.

Figure 65 shows the variation of $\Delta_{mix}G$ of mixed POPE:CL monolayers as a function of the molar fraction of CL at different surface pressures.

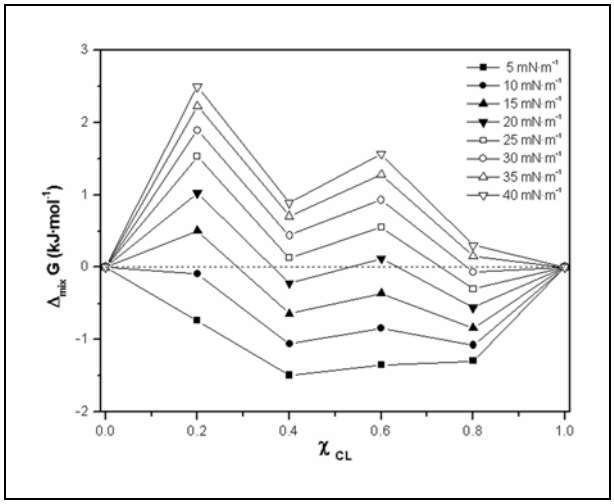

Figure 65. Variation of the Gibbs energy of mixing with the molar fraction of CL at different surface pressures.

Neither the maximum nor the minimum points of the positive and negative $\Delta_{mix}G$ values are well defined in the plot. When $\pi \leq 20$ mN·m^{-1}, the values of $\Delta_{mix}G$ are negative in almost all molar fractions, but when $\pi > 20$ mN·m^{-1}, the values of $\Delta_{mix}G$ are positive. Positive and negative $\Delta_{mix}G$ values indicate stability and instability in the monolayer, respectively. At low surface pressures attractive forces appear between phospholipid molecules but the same effect is not observed at higher surface pressures due to two effects: a steric effect at small CL molar fractions and charge repulsion at high CL molar fractions.

For all ranges of CL molar fraction assayed, $\Delta_{mix}G$ values increase when the surface pressure is increased. This can be attributed to the proximity of CL molecules when surface pressure is increased during lateral compaction.

V.1.3. POPE monolayer

Isotherms evaluated in this work identify POPE as the only pure phospholipid that shows a definite phase transition. To evaluate the nature of this phase transition POPE monolayers were studied at different temperatures.

V.1.3.1. POPE isotherms at different temperatures

Isotherms were performed at six different temperatures between 11 ºC and 37 ºC. Figure 66 shows a plot of the variation of the surface pressure of pure POPE as a function of the area per molecule at different temperatures.

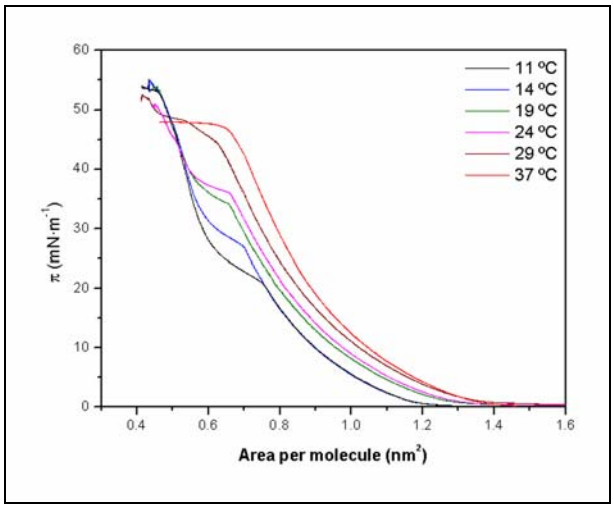

Figure 66. Isotherms of pure POPE at different temperatures.

It can be seen that POPE monolayer exhibits the LC-LC' transition at temperatures below 37 ºC. The onset point of transition is not fixed and depends on the temperature; at 11 ºC it occurs at a surface pressure of almost 21 $mN \cdot m^{-1}$ while at 24 ºC it is reached at a surface pressure of 36 $mN \cdot m^{-1}$.

Collapse surface pressure also changes with temperature. When the temperature is below 19 ºC the collapse pressure is approximately 53.5 $mN \cdot m^{-1}$. Above this temperature it decreases to values of 51 $mN \cdot m^{-1}$. Finally, at the highest temperature assayed, collapse is observed at almost 47.8 $mN \cdot m^{-1}$. This behaviour reflects the progressive disappearance of the LC-LC' transition.

Moreover, the area per molecule of pure POPE monolayer increases with temperature. For example, at a constant surface pressure of 10 $mN \cdot m^{-1}$ and before any transition has occurred, the monolayer at 11 ºC shows an area per molecule of ~ 0.90 nm^2, while the monolayer at 37 ºC shows an area per molecule of ~ 1.05 nm^2.

Another interesting feature in Figure 66 is the position of the second transition. This second transition is very subtle and has a surface pressure of ~ 45 $mN \cdot m^{-1}$ for monolayers acquired at temperatures below 29 ºC. The transition becomes more pronounced in the monolayer at 29 ºC, with a mean surface pressure of 48.4 $mN \cdot m^{-1}$, and disappears for the monolayer acquired at 37 ºC.

V.1.3.2. Compressibility modulus

To analyze the physical properties of POPE monolayers at different temperatures the compressibility modulus was calculated according equation IX. Figure 67 shows the variation of the surface pressure as a function of the compressibility modulus at different temperatures.

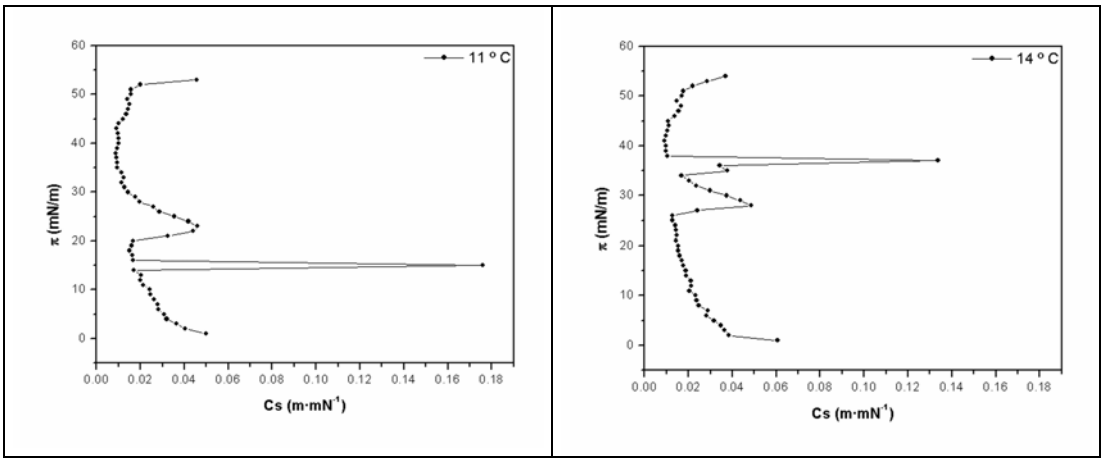

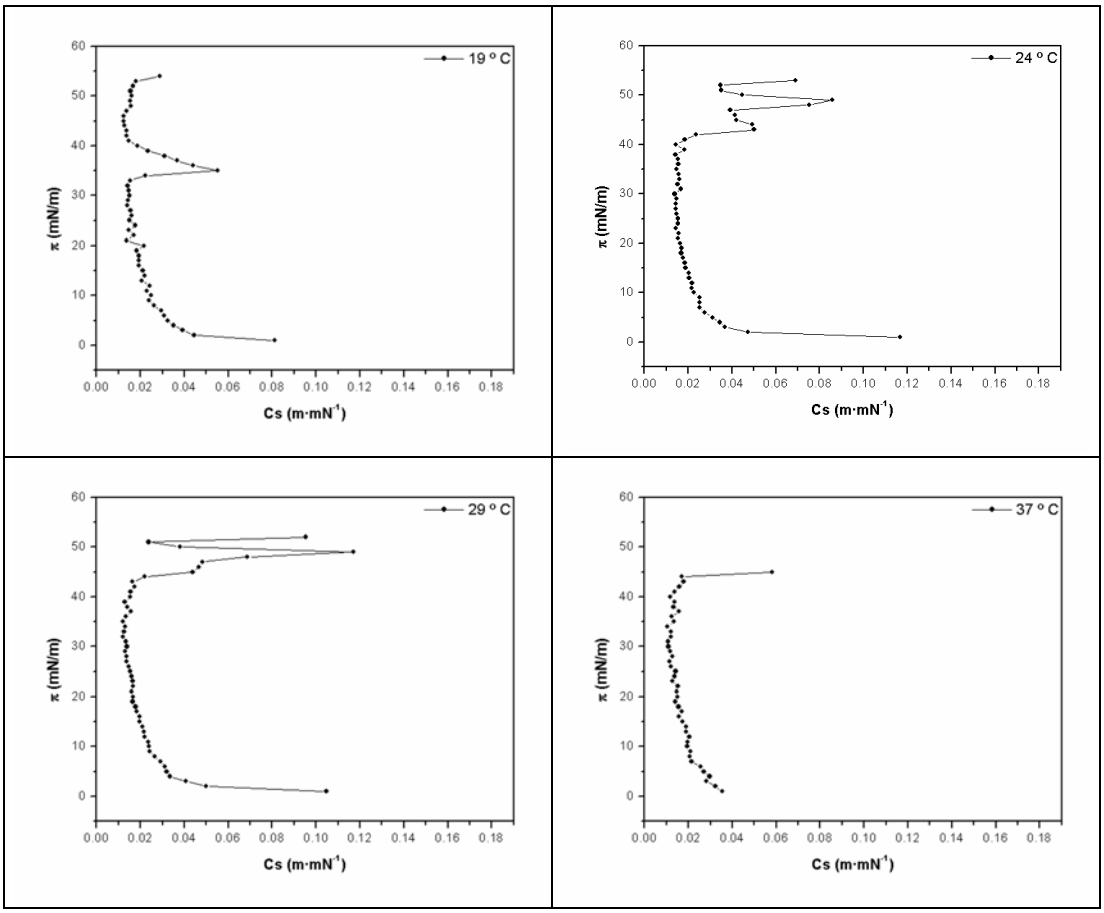

Figure 67. Compressibility modulus of POPE monolayers at different temperatures.

All POPE monolayers present very similar C_s basal values. In the monolayer acquired at 37 ºC the value of C_s is almost constant and continuous when the surface pressure is modified, but for temperatures below 37 ºC the compressibility modulus undergoes some changes. Two peaks appear in all monolayers except for the monolayer at 19 ºC, in which only one peak is present. One is a sharp peak whose C_s value decreases when temperature is increased; the other peak is wider and presents similar values of C_s before and after the transition point. The LC-LC' transition causes the wider peak while sharp peak can be attributed to the second transition appearing in the monolayers in Figure 66. It is interesting that the wide peak is present in all monolayers below 37 ºC, but the sharp peak does not appear in the monolayer acquired at 19 ºC. Moreover, at 11 ºC the sharp peak appears at a lower surface pressure than the wide peak, but above this temperature the wide peak always appears at lower surface pressures than the sharp peak. In the monolayer at 29 ºC peaks are in between each other.

V.1.3. *Cyt c* adsorption to monolayers

Adsorption experiments were carried out with pure phospholipids and with the more stable monolayers (identified by the Gibbs energy tests) that contain CL. As described in the introduction, *cyt c* can be specified linked to CL molecules.

Adsorption isotherms were performed as described in section IV.2.7. at 24 ºC. This temperature was selected because the monolayers showed greater reproducibility at 24 ºC than at 37 ºC. Monolayers of the desired composition were compressed to a surface pressure of 30 $mN \cdot m^{-1}$ and *cyt c* was injected under the monolayer through the injection port.

V.1.4.1. Monolayers composed of POPC and CL

Figure 68 shows the variation in the increase of area per molecule due to *cyt c* incorporation into the monolayer as a function of time for pure POPC, pure CL and the most thermodynamically stable mixture of the two at 24 ºC.

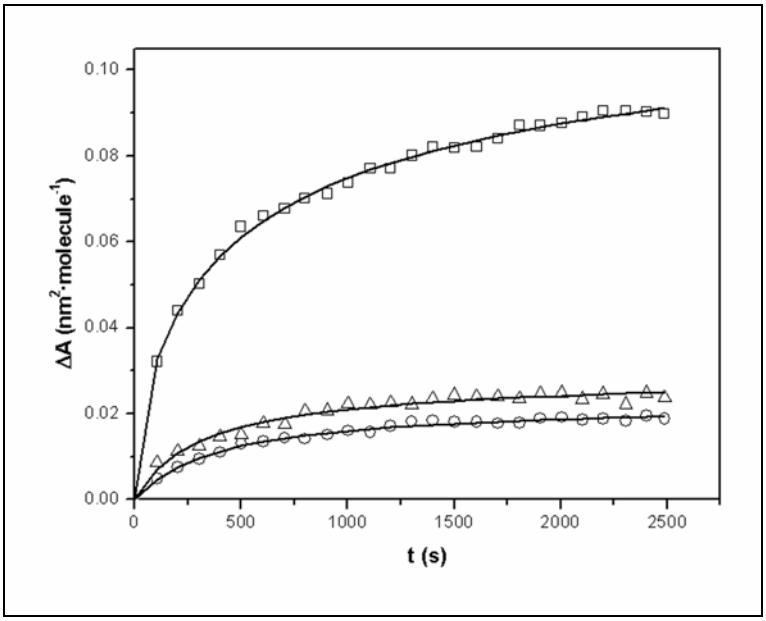

Figure 68. Variation of the molecular area due to *cyt c* adsorption to monolayers of POPC (△), POPC:CL (0.6:0.4, mol:mol) (○) and CL (□).

All monolayers assayed show a progressive increase of area per molecule due to *cyt c* adsorption. The cardiolipin monolayer gives the highest ΔA value while the POPC and

POPC:CL (0.6:0.4, mol:mol) monolayers show a similar response to *cyt c* adsorption and lower ΔA values than CL.

Experimental data were adjusted to equation X and the mathematical parameters are summarized in Table XI.

Table XI. Parameters from equation X for monolayers composed of POPC and CL.

	Monolayer composition		
	POPC	**POPC:CL (0.6:0.4, mol:mol)**	**CL**
ΔA_{max} ($nm^2 \cdot molecule^{-1}$)	2.9 ± 0.2	2.23 ± 0.09	12.9 ± 0.5
k x 10^{-3} (s^{-1})	2.8 ± 0.5	2.5 ± 0.2	1.7 ± 0.2
b	0.91 ± 0.13	1.00 ± 0.09	0.67 ± 0.03

The pure CL monolayer shows the highest ΔA_{max} value while the mixture of POPC and CL gives the lowest. This suggests that the CL monolayer displays the highest *cyt c* adsorption while the mixed monolayer shows the lowest protein adsorption. The POPC and lipid mixture shows higher values of k and b than pure CL, indicating that *cyt c* molecules are adsorbed more rapidly to monolayers containing POPC than to pure CL.

V.1.4.2. Monolayers composed of POPE and CL

Figure 69 shows the variation in the increase of area per molecule due to *cyt c* incorporation to the monolayer as a function of time for pure POPE, pure CL and the most thermodynamically stable mixture of the two at 24 ºC.

All monolayers assayed show a progressive increase of area per molecule due to *cyt c* adsorption. The CL monolayer gives the highest ΔA value while the POPE monolayer gives the lowest. The POPE:CL (0.8:0.2, mol:mol) mixed monolayer shows an intermediate response to *cyt c* adsorption between the two pure phospholipids. In this case POPE behaves similarly to POPC in *cyt c* adsorption experiments: both are zwiterionic phospholipids and show a lesser response than monolayers containing CL. The mixed monolayer, despite the small CL molar fraction in its composition, shows high ΔA values.

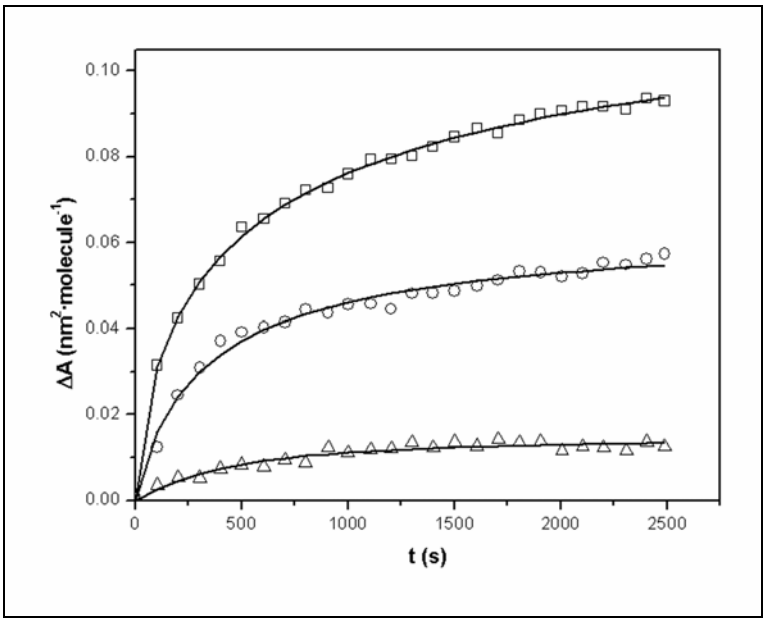

Figure 69. Variation of the molecular area due to *cyt c* adsorption to monolayers of POPE (△), POPE:CL (0.8:0.2, mol:mol) (○) and CL (□).

Experimental data were adjusted to equation X and the mathematical parameters are summarized in Table XII.

Table XII. Parameters from equation X for monolayers composed of POPE and CL.

	Monolayer composition		
	POPE	**POPE:CL (0.8:0.2, mol:mol)**	**CL**
ΔA_{max} ($nm^2 \cdot molecule^{-1}$)	1.49 ± 0.13	6.4 ± 0.3	12.9 ± 0.5
k x 10^{-3} (s^{-1})	2.5± 0.5	2.9 ± 0.4	1.7 ± 0.2
b	1.2 ± 0.3	0.91 ± 0.11	0.67 ± 0.03

The pure CL monolayer shows the highest ΔA_{max} value while pure POPE shows the lowest. Although the proportion of CL in the mixture is low, the ΔA_{max} values given by the mixed monolayer are almost half those of pure CL. This suggests that an atypical distribution of molecules in the monolayer allows the adsorption of a higher proportion of *cyt c* than the mixed POPC and CL monolayer. The POPE and lipid mixture shows similar values of *k* and *b* while pure CL presents lower *k* and *b* values than the other two monolayers assayed, which indicates that *cyt c* molecules are adsorbed more rapidly to monolayers containing POPE than to pure CL.

V.2. AFM LB FILM CHARACTERIZATION

LB films were extracted as described in section IV.2.8. on freshly cleaved mica. All films were scanned in air and in contact mode.

V.2.1. POPC LB film

Figure 70 shows AFM images of two POPC LB films at different values of surface pressure.

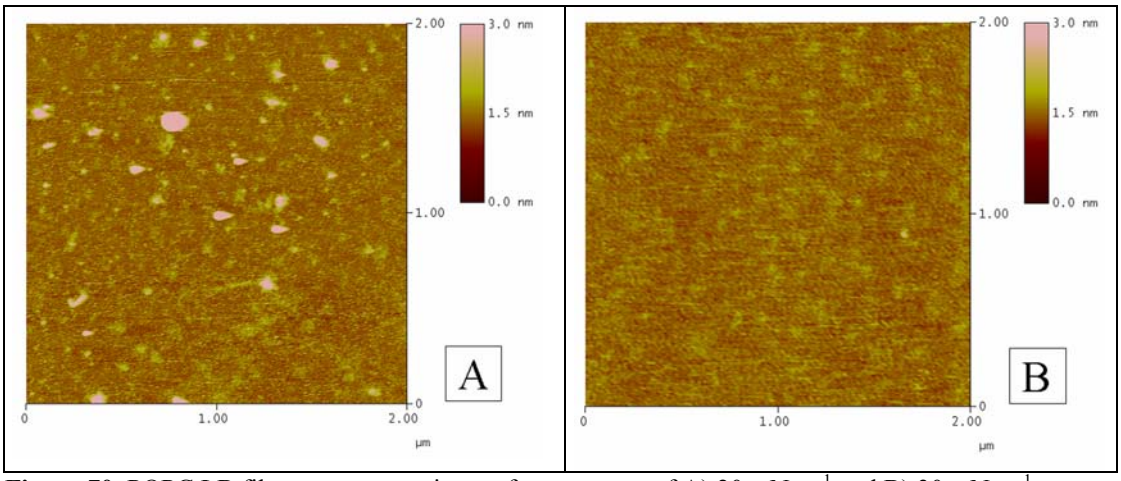

Figure 70. POPC LB films at an extraction surface pressure of A) 20 $mN \cdot m^{-1}$ and B) 30 $mN \cdot m^{-1}$.

Figure 70A shows a POPC LB film at a surface pressure of 20 $mN \cdot m^{-1}$, in the LE state of this phospholipid. The height of this LB taking the mica as a reference is 0.27 nm. LB film height was inferred by scratching the monolayer with the AFM tip. The image reveals some kind of protrusion: white structures with diameters of ~ 70 nm and heights between 2.00 nm and 2.50 nm. These protrusions could be caused by lipid aggregation on the LB film surface. The POPC LB film covers the entire mica substrate and has a mean roughness (*Ra*) of 0.06 nm. This LB film exhibits some sort of higher structure that covers 19% of its total surface measured using the bearing analysis feature of Nanoscope® software. This region is seen in the image as a blurred yellow structure.

Figure 70B shows a POPC LB film extracted at a surface pressure of 30 $mN \cdot m^{-1}$, also in the LE state. The height of this LB film above the mica surface is 0.42 nm. The topography of this image is very similar to that of the image in Figure 70A, but the

protrusions are not observed in this case. The monomolecular film gives a mean *Ra* value of 0.10 nm. Molecules in the monolayer at a surface pressure of 30 $mN \cdot m^{-1}$ are restricted to a smaller area per molecule, giving the monolayer a greater packing density than at 20 $mN \cdot m^{-1}$. This proximity between adjacent molecules can prevent the deformation of monolayer caused by the tip scan. In this image the yellow structure defined above, which now cover nearly 40% of the surface of the image shown, is clearly seen. Force spectroscopy reveals that the POPC LB film at a surface pressure of 30 $mN \cdot m^{-1}$ could have a mean height of ~ 2 nm.

V.2.2. CL LB film

Figure 71 shows two AFM images of CL LB films at two different values of surface pressure.

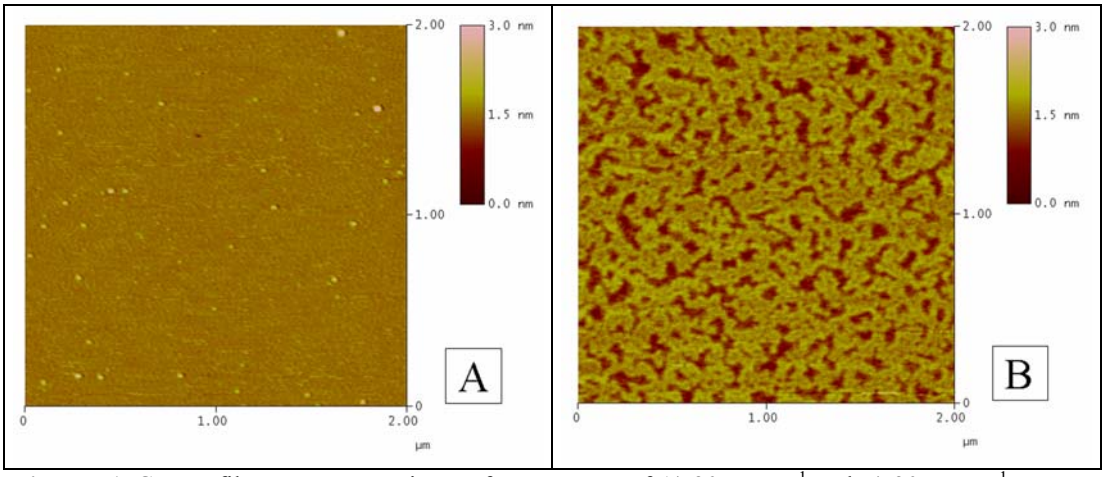

Figure 71. CL LB films at an extraction surface pressure of A) 20 $mN \cdot m^{-1}$ and B) 30 $mN \cdot m^{-1}$.

Figure 71A shows a CL LB film at a surface pressure of 20 $mN \cdot m^{-1}$. From this image it can be seen that the monolayer covers the entire mica surface and that some lipid aggregates are present.

Figure 71B shows a CL LB film at a surface pressure of 30 $mN \cdot m^{-1}$. In this image two different structures can be distinguished, with a step height difference of 0.90 nm and an *Ra* value for the upper structure of 0.09 nm. The lower structure has a two-dimensional channel-like arrangement due to the compaction caused by the upper structure.

V.2.3. POPE LB film

Figure 72 shows two AFM images of POPE LB films at two different values of surface pressure.

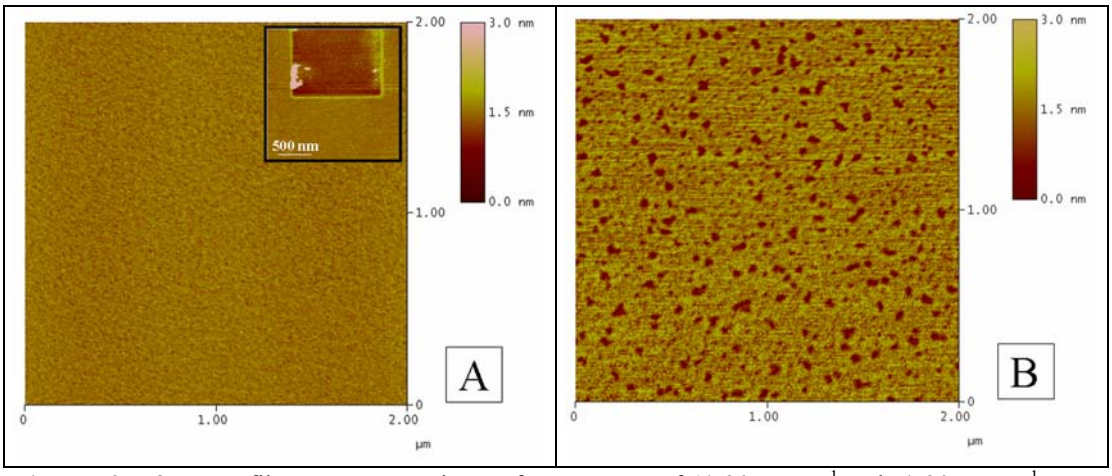

Figure 72. POPE LB films at an extraction surface pressure of A) 20 $mN \cdot m^{-1}$ and B) 30 $mN \cdot m^{-1}$.

Figure 72A shows a POPE monolayer at a surface pressure of 20 $mN \cdot m^{-1}$. The inset shows a square of ~ 1 μm^2 scratched with the AFM tip to measure the height of the monolayer. The step height difference between the mica surface and the top of the monolayer is 0.30 nm. The mean *Ra* value of the surface of the monolayer is 0.05 nm. It is significant that the *Ra* value of 0.04 nm for the uncovered mica is quite similar to the *Ra* value of the monolayer. As expected, after scratching the monolayer, lipid accumulations can be found at the edges of the square with heights of more than 4 nm over the monolayer. No lipid aggregates are found on monolayer surface, suggesting that at this surface pressure the monolayer is not eroded during the scan.

Figure 72B shows a POPE monolayer extracted at a surface pressure of 30 $mN \cdot m^{-1}$. In this image small, round depressions can be seen in the LB film. These depressions have mean diameters of ~ 75 nm and measure 1.16 nm in depth from the monolayer surface. In this case, the POPE monolayer has a *Ra* value of 0.14 nm, which is three times the *Ra* value of the monolayer at a surface pressure of 20 $mN \cdot m^{-1}$. Force spectroscopy showed that for the POPE LB film at a surface pressure of 30 $mN \cdot m^{-1}$ there is no jump in the approaching force curve, so the monolayer height could not be inferred from

force spectroscopy. As in the case of the monolayer at 20 $mN \cdot m^{-1}$, no lipid aggregates are found on the monolayer surface.

Given the characteristic, well-pronounced transition of the POPE monolayer at 36 $mN \cdot m^{-1}$ and the information provided by AFM in the visualization of LB films, a more exhaustive study was performed close to this surface pressure. Figure 73 shows the AFM images of a POPE LB film at a surface pressure of 36.5 $mN \cdot m^{-1}$ – 0.5 $mN \cdot m^{-1}$ above the LC-LC' transition.

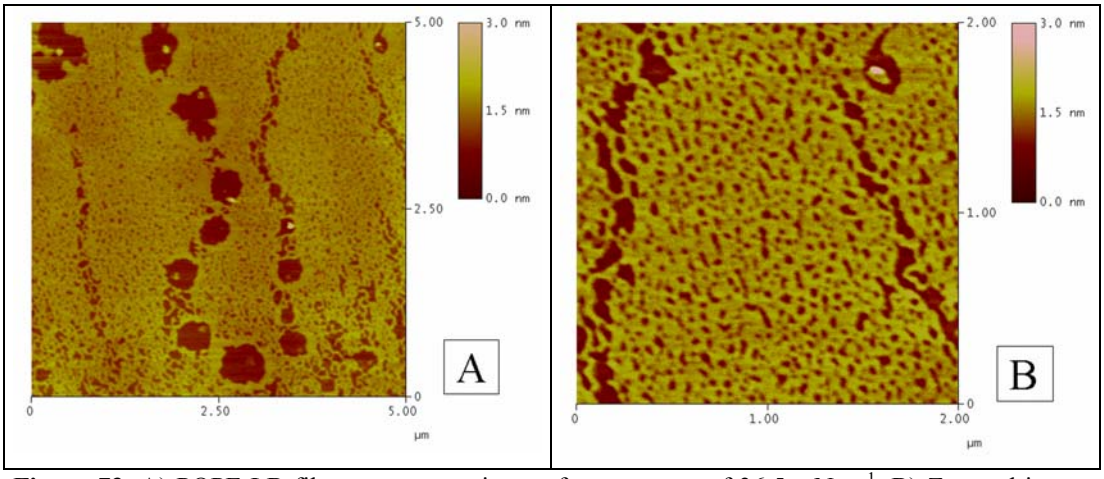

Figure 73. A) POPE LB film at an extraction surface pressure of 36.5 $mN \cdot m^{-1}$. B) Zoomed image from A.

Figure 73A shows a film covering the mica surface with large, round structures that break the homogeneity of the layer. The height of this monolayer is 0.80 nm and the *Ra* value is 0.16 nm. Two types of round structure with mean diameters of 500 nm and 90 nm can be seen. Interestingly, the round structures are aligned and form fissures in the monolayer.

Figure 73B shows a zoomed image from Figure 73A. In this image a region between two fissures can be seen that is quite similar to Figure 72B. The small, round structures in this region have mean diameters of ~ 50 nm and a mean height of 1.12 nm.

Figure 74A shows a topographic image of the POPE LB film at a surface pressure of 36.5 $mN \cdot m^{-1}$ where a 1 μm^2 square has been scratched with the AFM tip. Sharp edges are found at the end of the scratched zone and lipid structures appear randomly distributed at the bottom edge of the scratched region. From the section analysis, shown

in Figure 74B, it can be seen that the larger round structures have a similar height to the scratched zone while the smaller structures do not reach the bare mica surface. It is necessary to bear in mind that, for small structures such as those observed here, the tip may not reach the bare mica surface because the diameter of these structures is close to the diameter of the tip. Interestingly, the scratched zone is not completely flat and has an *Ra* value of 0.07 nm.

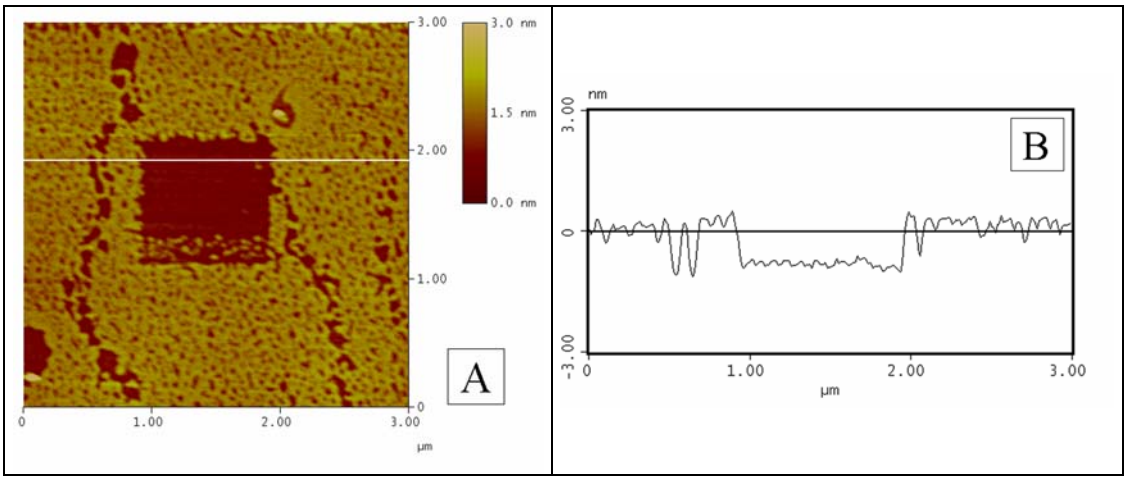

Figure 74. A) POPE LB film scratched monolayer and B) section analysis of image A.

Figure 75 shows a POPE LB film at a surface pressure of 39 $mN \cdot m^{-1}$, above the so so-named LC-LC' transition.

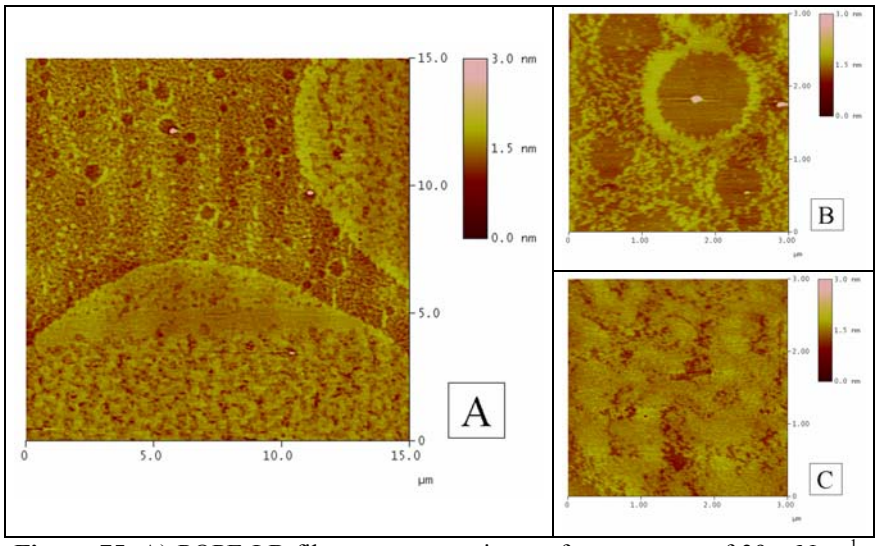

Figure 75. A) POPE LB film at an extraction surface pressure of 39 $mN \cdot m^{-1}$, B) zoomed image of the lower structure and C) zoomed image of the higher structure.

Figure 75A exhibits two different regions: one of lower height that is formed by a monolayer with large round structures (Figure 75B); and a second, higher region that is more condensed (Figure 75C) and shows clearly defined edges with the other region. To obtain the height of the LB film the monolayer was scratched with the AFM tip. The step height measurement from the bare mica surface to the region inside the large round structures is negligible (less than the *Ra* of mica surface); the height between the bare mica and the region that forms these circles is 1.19 nm and the height between the region that forms the circles and the condensed structure is 0.63 nm. With these height measures the taller region can be formed due to the lateral compactness of the lower structures towards a more condensed structure.

Figure 76 shows the AFM images (150 x 150 μm^2) of the LB film shown in Figure 75A.

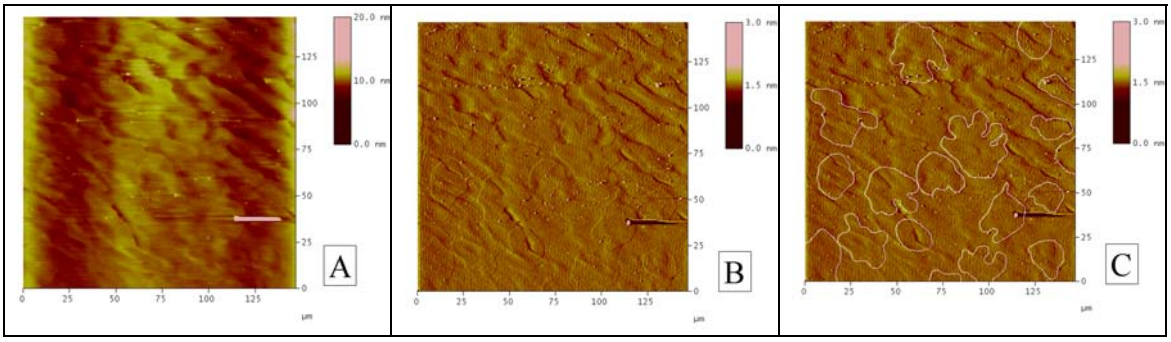

Figure 76. High scan of POPE monolayer A) topographic image B) deflection image and C) false edges of condensed structure in image B.

Figure 76A shows the topographic image but no structures can be clearly identified due to the limited piezoelectric scan. Figure 76B shows the deflection image of 76A in which the condensed structures can be seen. Figure 76C shows the same image as in Figure 76B but the edges of the condensed structures have been highlighted to make them easier to identify. Each structure has a diameter greater than 25 μm. These condensed structures are not uniformly distributed in the LB film and have several different sizes and shapes.

V.2.3.1. BAM characterization of POPE monolayer

BAM was used to characterize the POPE monolayer under the same experimental conditions used for the isotherms and LB films. Figure 77 shows three BAM images at three different surface pressures.

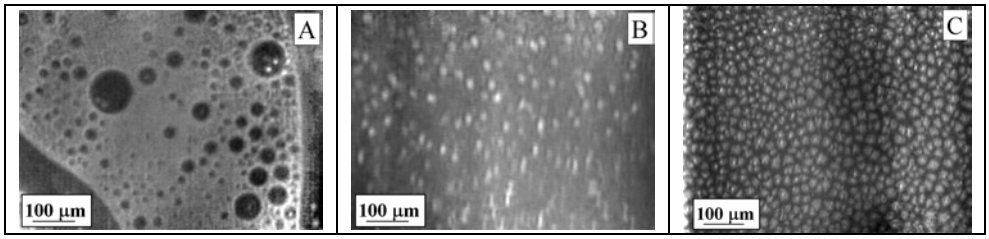

Figure 77. BAM images of POPE monolayer at different surface pressures A) 0.5 $mN \cdot m^{-1}$, B) 20 $mN \cdot m^{-1}$ and C) 45 $mN \cdot m^{-1}$.

Figure 77A shows the POPE monolayer at a surface pressure of 0.5 $mN \cdot m^{-1}$. In this image the darkest region corresponds to the monolayer in a gas phase while the brightest structure is the monolayer in the LE phase. In Figure 77B, at ~ 20 $mN \cdot m^{-1}$, the gas phase has vanished and a new, brighter structure appears. In this image the background is the LE phase of the POPE monolayer while the new structures are more condensed structures. In Figure 77C, at ~ 45 $mN \cdot m^{-1}$, a new phase appears as bright spots using the structures in Figure 77B as nucleation points. In this last image the darkest region is the POPE monolayer in the LE phase while the other structures are molecules in a more condensed phase. These structures have mean diameters of ~ 30 μm.

Figure 78 shows two images of the POPE monolayer. AFM and BAM images are displayed on a POPE isotherm indicating the surface pressure of the observation. Although the BAM and AFM images are not at the same surface pressures and the techniques work for different lateral dimensions, it becomes apparent that at high surface pressures both techniques identify the condensed structure of the POPE monolayer. It is worth noting that the magnifications of the images are different.

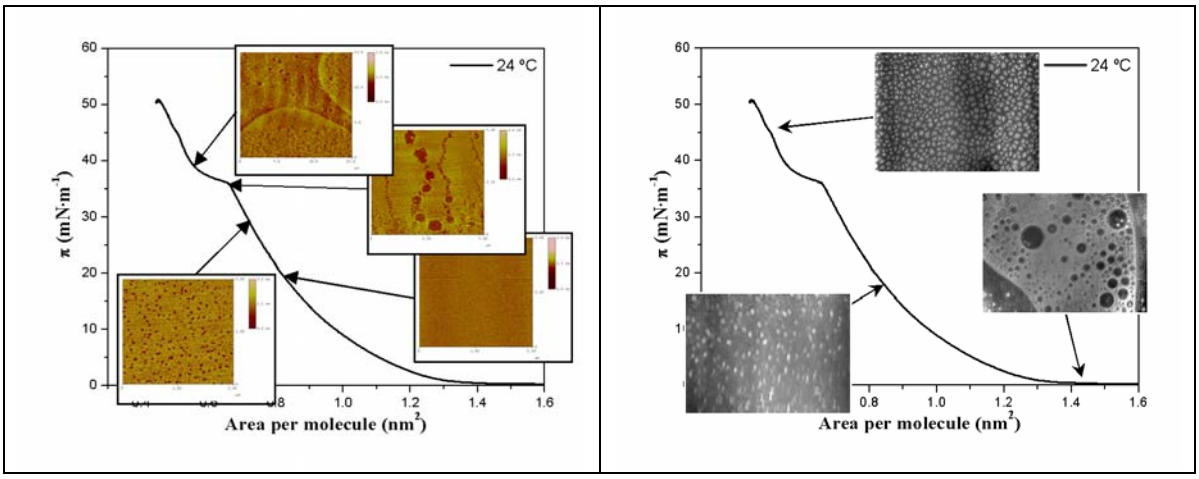

Figure 78. Images of POPE monolayer A) AFM images and B) BAM images.

V.2.4. LB films of lipid mixtures

V.2.4.1. POPE:POPC (0.6:0.4, mol:mol)

Figure 79 shows two AFM images of POPE:POPC (0.6:0.4, mol:mol) LB films at two different values of surface pressure.

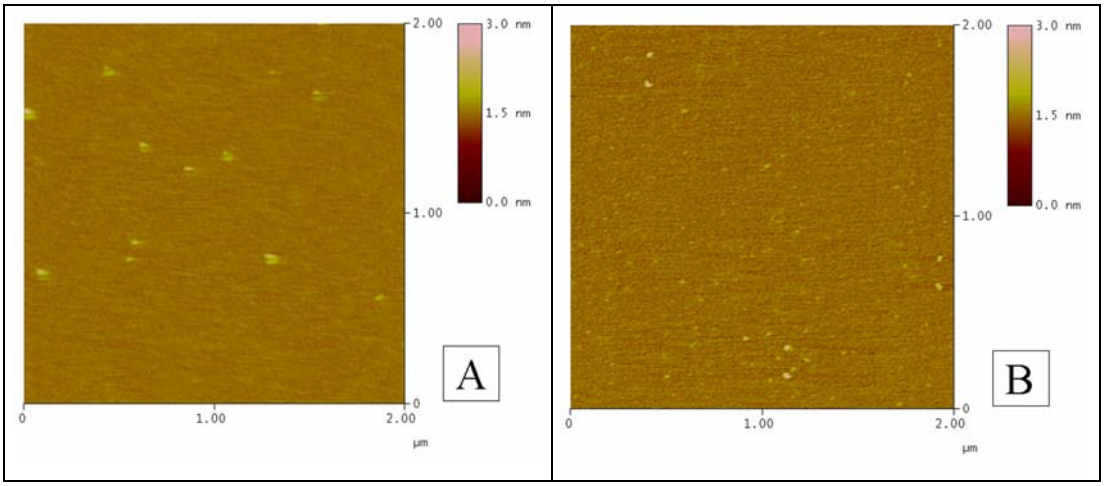

Figure 79. POPE:POPC (0.6:0.4, mol:mol) LB films at extraction surface pressures of A) 20 $mN \cdot m^{-1}$ and B) 30 $mN \cdot m^{-1}$.

Figure 79A shows a POPE:POPC (0.6:0.4, mol:mol) LB film at a surface pressure of 20 $mN \cdot m^{-1}$. In this image the monolayer covers the entire mica surface with a mean *Ra* value of 0.05 nm and higher, round protrusions are visible. These structures have similar features and their mean diameters are ~ 50 nm and 0.67 nm taller than the flat surface of the monolayer. As described in previous sections, these protrusions are attributed to lipid aggregation on the monolayer surface.

Figure 79B shows a POPE:POPC (0.6:0.4, mol:mol) LB film at a surface pressure of 30 $mN \cdot m^{-1}$ that covers the entire substrate. The monolayer has the same *Ra* value as the monolayer at a surface pressure of 20 $mN \cdot m^{-1}$, which is 0.05 nm. In this LB film there are a smaller number of protrusions over the monolayer surface, which are of similar height and have diameters of ~ 30 nm. Force spectroscopy showed that the POPE:POPC (0.6:0.4, mol:mol) LB film at a surface pressure of 30 $mN \cdot m^{-1}$ has a mean height of ~ 2 nm.

V.2.4.2. POPC:CL (0.6:0.4, mol:mol)

Figure 80 shows two AFM images of POPC:CL (0.6:0.4, mol:mol) LB films at two different values of surface pressure.

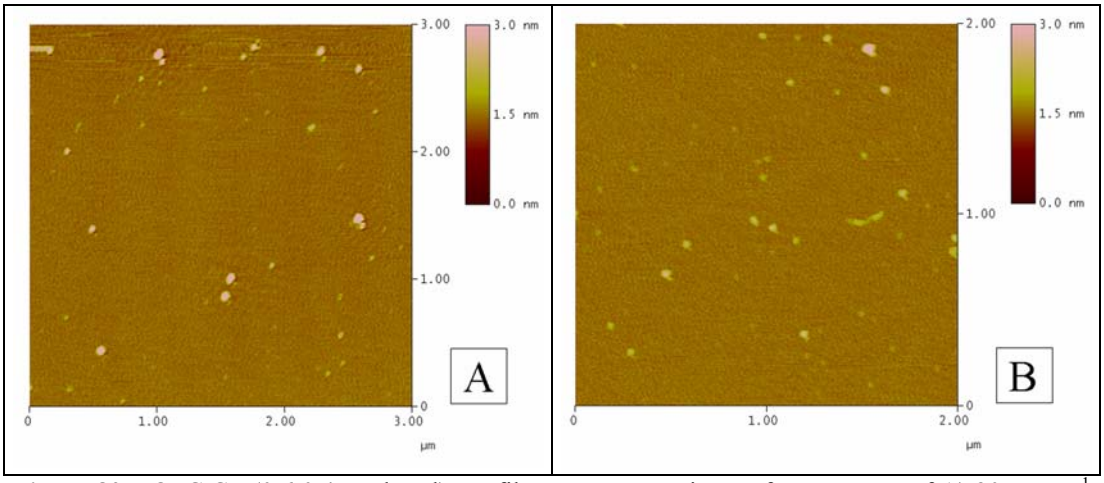

Figure 80. POPC:CL (0.6:0.4, mol:mol) LB films at an extraction surface pressure of A) 20 $mN \cdot m^{-1}$ and B) 30 $mN \cdot m^{-1}$.

Figures 80A and 80B show two POPC:CL (0.6:0.4, mol:mol) LB films at surface pressures of 20 and 30 $mN \cdot m^{-1}$, respectively. The images are very similar and present a whole LB film that covers the mica surface. In both images the protrusions are clearly visible on the monolayer and are taller and wider in Figure 80A than in Figure 80B.

V.2.4.3. POPE:CL (0.8:0.2, mol:mol)

Figure 81 shows two AFM images of the POPE:CL (0.8:0.2, mol:mol) LB film at two different values of surface pressure.

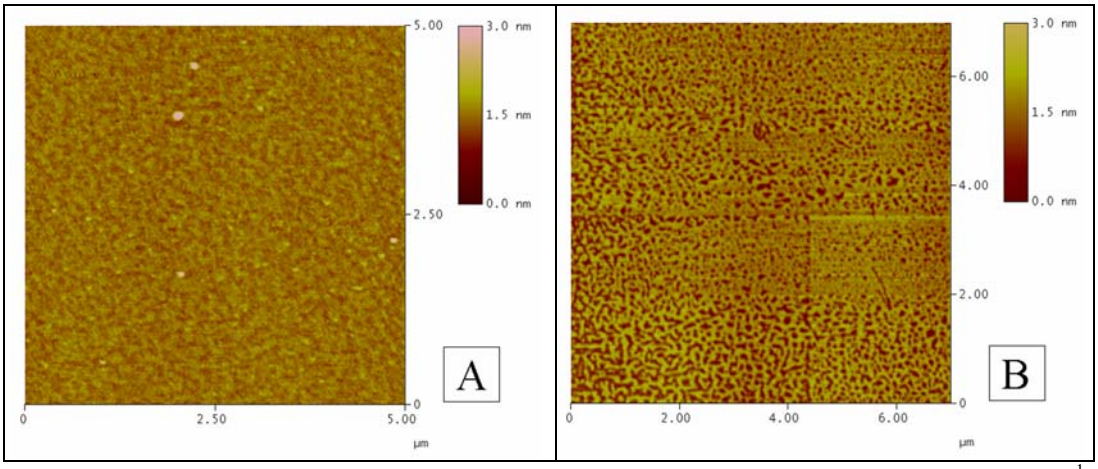

Figure 81. POPE:CL (0.8:0.2, mol:mol) LB films at extraction surface pressures of A) 20 $mN \cdot m^{-1}$ and B) 30 $mN \cdot m^{-1}$.

Figure 81A shows the POPE:CL (0.8:0.2, mol:mol) monolayer extracted at a surface pressure of 20 $mN \cdot m^{-1}$. The monolayer covers the whole mica surface with a mean *Ra* value of 0.11 nm and some protrusions are visible on the monolayer surface. From this image it can be seen that monolayer has a type of two-dimensional arrangement with uniform distribution.

Figure 81B shows a POPE:CL (0.8:0.2, mol:mol) LB film at a surface pressure of 30 $mN \cdot m^{-1}$. In this image two different regions can be seen, with a step height of 1.33 nm between them. Interestingly, the upper structure appears to show different two-dimensional arrangements in different regions.

Figure 82 shows a magnification of the image in Figure 81B. It can be seen that the monolayer may adopt different structures. In the white square the upper structure forms a channel-like framework, while in the white rectangle the upper structure is more compacted and encloses a dark region with small round structures. This random distribution could be caused by phase separation in the different regions of the mixed monolayer.

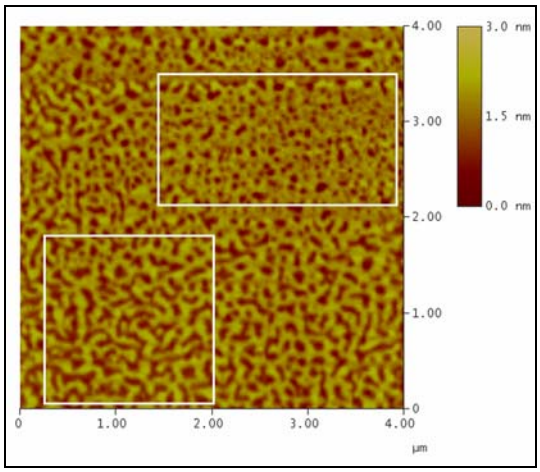

Figure 82. Zoomed image from Figure 81B in which two different lipid arrangements are indicated.

V.2.4.4. POPE:POPC:CL (0.5:0.3:0.2, mol:mol:mol)

Figure 83 shows two AFM images of POPE:POPC:CL (0.5:0.3:0.2, mol:mol:mol) LB films at two different values of surface pressure.

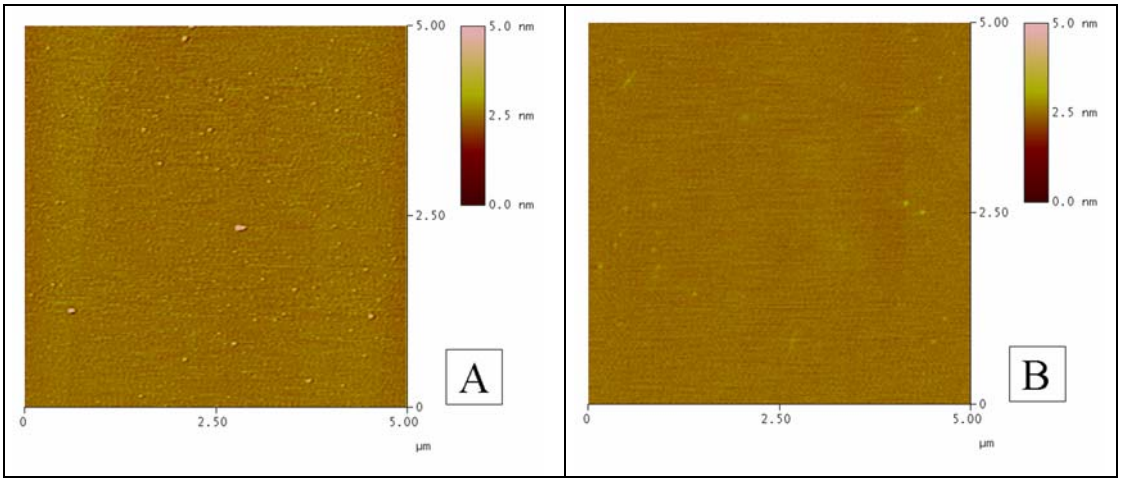

Figure 83. POPE:POPC:CL (0.5:0.3:0.2, mol:mol:mol) LB films at an extraction surface pressures of A) 20 $mN \cdot m^{-1}$ and B) 30 $mN \cdot m^{-1}$.

Figure 83A shows a POPE:POPC:CL (0.5:0.3:0.2, mol:mol:mol) LB film at a surface pressure of 20 $mN \cdot m^{-1}$ in the LE state with a height of 0.35 nm over the mica surface and a mean *Ra* value of 0.20 nm. The monolayer height was inferred by scratching the monolayer with the AFM tip. In this image, protrusions are visible on the LB film surface: white structures with diameters of ~ 30 nm. The protrusions on the monolayer

surface could be lipid aggregation or atmospheric contaminants as the samples were scanned in air.

Figure 83B shows a POPE:POPC:CL (0.5:0.3:0.2, mol:mol:mol) LB film at a surface pressure of 30 $mN \cdot m^{-1}$ in the LE state with a height of 0.50 nm over the mica surface. This image is very similar to the one in Figure 83A, where no protrusions are visible. The image has an *Ra* value of 0.10 nm. The molecules in this monolayer are compacted because the surface pressure is greater than for the monolayer shown in Figure 83A. This gives the monolayer greater stability against tip deformation during scans preventing the formation of lipid aggregates.

V.3. FLUORIMETRIC SURFACE STUDIES

V.3.1. Transition temperature of mixed liposomes

The transition temperatures of mixed liposomes were obtained by monitoring the fluorescence anisotropy of DPH against temperature as described in the Experimental Methods section. Figure 84 shows the variation of *r* as a function of temperature for the mixed liposomes used in this study.

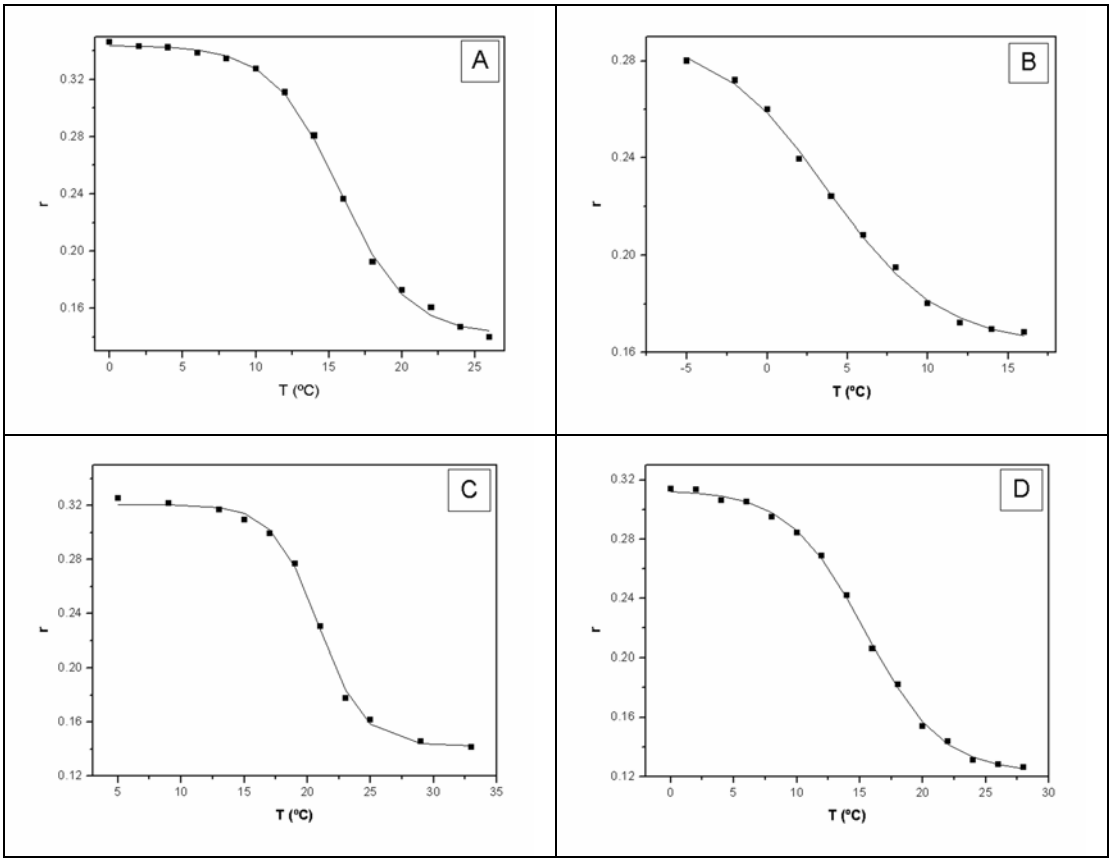

Figure 84. Variation of fluorescence anisotropy of DPH as a function of temperature for: A) POPE:POPC (0.6:0.4, mol:mol); B) POPC:CL (0.6:0.4, mol:mol); C) POPE:CL (0.8:0.2, mol:mol) and D) POPE:POPC:CL (0.5:0.3:0.20, mol:mol:mol).

All data show a well defined sigmoid behaviour that provides a satisfactory fit to equation XV, with mean values of R^2 no lower than 0.999.

Table XIII summarizes the parameters obtained from the data adjustment of Figure 84 to equation XV and the transition temperature (T_m) of pure phospholipids. It can be seen from the table that the ternary mixture showed a similar transition temperature to lipid mixtures of POPE and POPC but with lower cooperativity. The POPE:CL and

POPC:CL mixtures have the highest and the lowest cooperativity value, respectively, of all samples studied.

Table XIII. Transition temperatures for mixed liposomes and pure phospholipids.

Lipid composition	T_m (ºC)	r_1	r_2	b
POPE:POPC (0.6:0.4, mol:mol)	15.73 ± 0.13	0.343 ± 0.002	0.142 ± 0.002	2.91 ± 0.14
POPC:CL (0.6:0.4, mol:mol)	4.0 ± 0.4	0.293 ± 0.006	0.157 ± 0.007	0.44 ± 0.07
POPE:CL (0.8:0.2, mol:mol)	20.82 ± 0.18	0.320 ± 0.002	0.144 ± 0.002	5.2 ± 0.4
POPE:POPC:CL (0.5:0.3:0.2, mol:mol:mol)	15.46 ± 0.15	0.313 ± 0.002	0.121 ± 0.003	2.19 ± 0.10
POPE*	25	-	-	-
POPC*	-2	-	-	-
CL#	19	-	-	-

V.3.2. ANS emission coefficients

The emission coefficients of ANS were measured and calculated as described in section IV.3.1.1. In Table XIV the coefficients for the different samples used in this study are summarized.

Table XIV. ANS emission coefficients at 24 ºC.

Sample	A_i (μM^{-1})
Buffer	1.2
POPC	287.0
POPE	71.4
CL	44.5
POPE:POPC (0.6:0.4, mol:mol)	154.5
POPC:CL (0.6:0.4, mol:mol)	50.1
POPE:CL (0.8:0.2, mol:mol)	28.4
POPE:POPC:CL (0.5:0.3:0.2, mol:mol:mol)	107.9
POPC:POPG (0.43:0.57, mol:mol)	78.0
POPE:POPG (0.66:0.33, mol:mol)	46.5

The emission coefficient observed in the buffer solution (50 mM Tris·HCl, 150 mM NaCl, *pH* 7.40), as expected, is the lowest. Samples containing POPC show higher

* From Avanti Polar Lipids (http://www.avantilipids.com)
# [Vasilenco et al., 1982]

emission coefficients than samples containing POPE and when CL is incorporated into the sample the value of the emission coefficient decreases. This could be the result of the negative charges brought by CL. These negative charges can induce repulsion with the fluorescent probe. In other words, ANS, an anionic molecule, may be less attached to samples when CL is present in the composition.

V.3.3. Surface electrostatic potential variation

V.3.3.1. *Cyt c* incubation time

To ensure the reproducibility of experiments a minimum incubation time of *cyt c* with liposomes was established. Figure 85 shows the decrease of fluorescence due to *cyt c* incorporation at a constant fluorescence probe concentration as a function of time for liposomes with two different lipid mixtures.

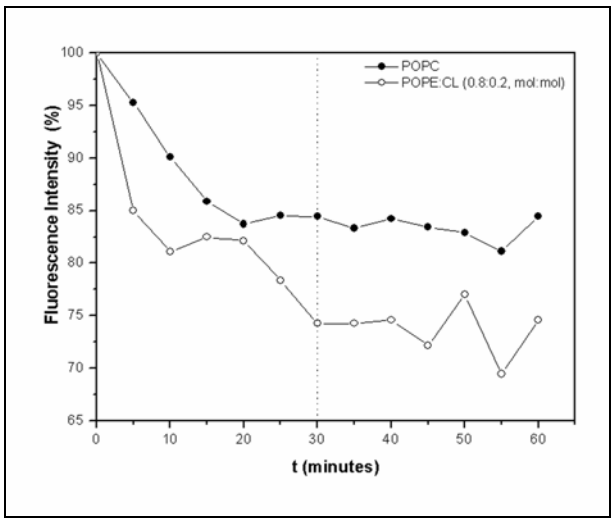

Figure 85. Variation of the fluorescence intensity due to *cyt c* incorporation as a function of incubation time.

In Figure 85 it can be seen that the fluorescence emission in both samples decreases considerably up to 30 minutes after the incorporation of *cyt c*. After this time, the variation of fluorescence is randomly distributed around a constant value. Interestingly, the decrease in fluorescence is greater in samples with CL than in pure POPC.

V.3.3.2. *Cyt c* concentration

The lipid to protein molar ratio (LPR_m) was evaluated before the incorporation of *cyt c* into liposomes could be analyzed. The decrease in fluorescence due to *cyt c* binding at a constant fluorescence probe concentration was monitored as a function of *cyt c* concentration in the sample.

Figure 86 shows the variation of the fluorescence emission due to *cyt c* incorporation as a function of LPR_m for four fluorescence probe concentrations.

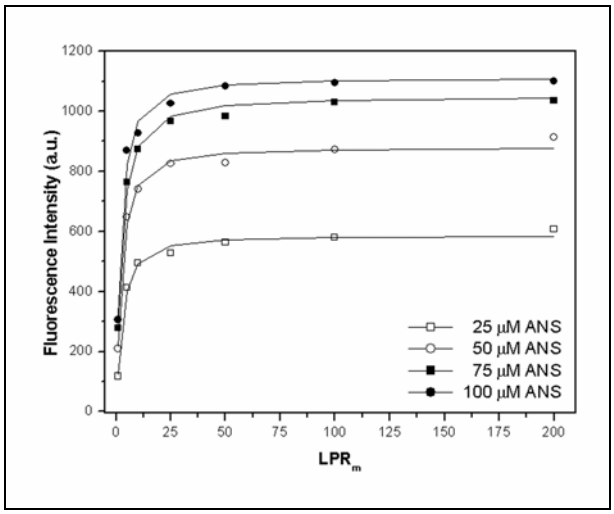

Figure 86. Variation of the fluorescence intensity due to *cyt c* incorporation as a function of LPR_m for four ANS molar concentrations.

As expected, the fluorescence intensity of the sample increases when the fluorescence probe concentration is increased. This increase is lower when the probe concentration is greater than 75 μM as the ANS binding sites become saturated. It is interesting to observe that the fluorescence emission is almost constant for a wide range of LPR_m values, from 200 to 25. At low LPR_m values, the fluorescence intensity decreases dramatically. As seen in all plots, the fluorescence intensity decreases considerably due to *cyt c* incorporation at $LPR_m \sim 15$. Interestingly, an LPR_m value of ~ 15 represents an LPR (weigh/weigh) value of ~ 1 for the lipid concentration used in the formation of liposomes.

V.3.3.3. Fluorescence variation due to *cyt c* incorporation

Samples for binding experiments were prepared as described in the Experimental Methods section. Figure 87 shows plots of the variation of fluorescence intensity emission with the successive addition of ANS to the sample for pure and mixed lipid compositions at 24 ºC. White and black squares represent samples with and without *cyt c*, respectively.

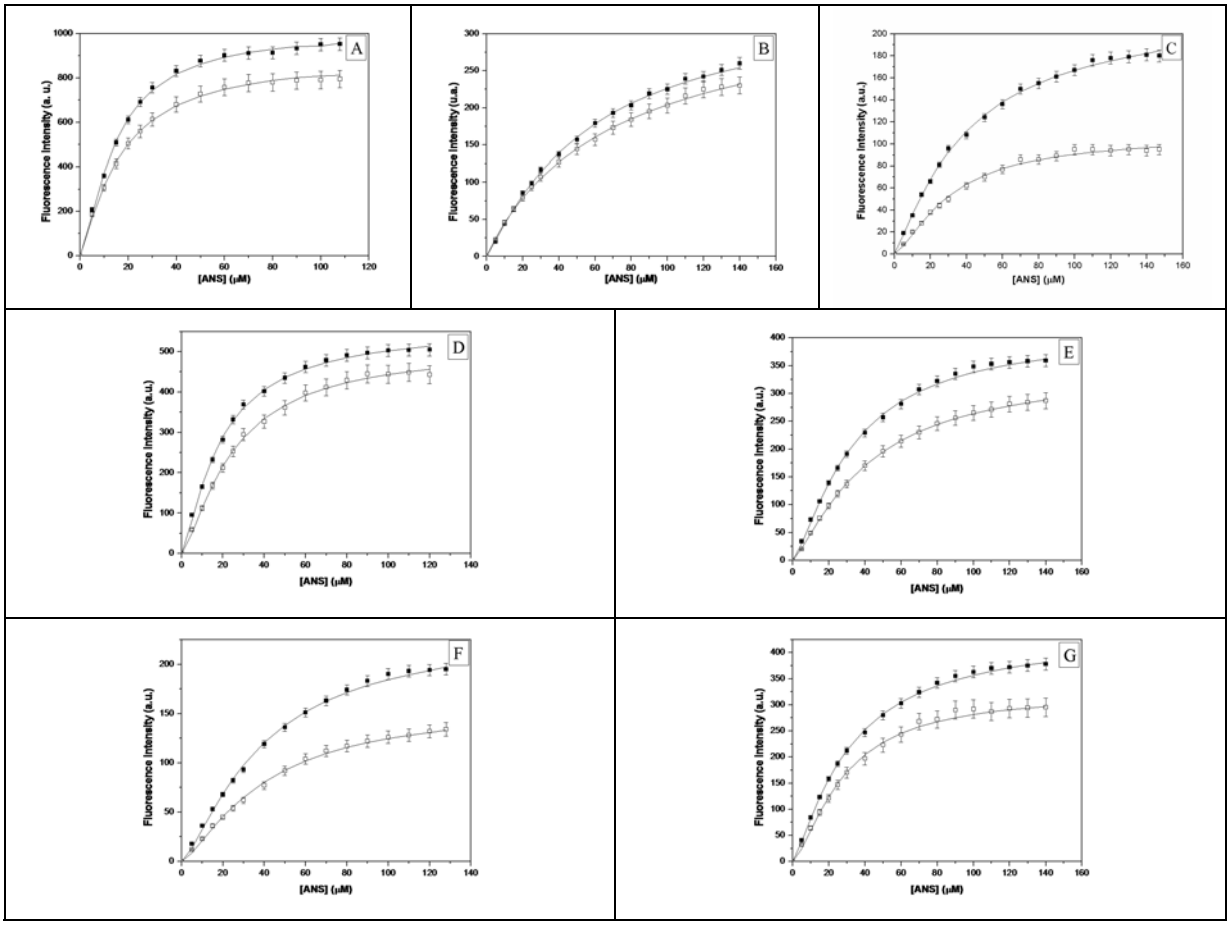

Figure 87. Fluorescence intensity variation as a function of ANS concentration for samples with (□) and without (■) *cyt c* for A) POPC, B) POPE, C) CL, D) POPE:POPC (0.6:0.4, mol:mol), E) POPC:CL (0.6:0.4, mol:mol), F) POPE:CL (0.8:0.2, mol:mol) and G) POPE:POPC:CL (0.5:0.3:0.2, mol:mol:mol).

In all experiments, reference samples (black squares) show higher fluorescence intensity than samples with incorporated *cyt c*. When the molecules of *cyt c* are adsorbed to liposomes the number of binding sites to which ANS binds is reduced. The difference in fluorescence intensity between the two curves is always greater than error bar values. This indicates that the decrease in fluorescence is mainly due to *cyt c*

adsorption. In the POPE experiment the error bars from both samples are close to each other but no overlapping is observed.

POPC samples show the maximum fluorescence intensity while corresponding values for samples in which POPE is the major phospholipid component are several times lower. The maximum and minimum differences in fluorescence intensity between the curves (measured as percentages) are observed for pure CL and pure POPE samples, respectively.

V.3.3.4. Surface electrostatic potential values

As explained in section IV.3.1.2., the variation of the surface electrostatic potential can be determined from the data in Figure 87 and with the ANS emission coefficients from Table XIV. Using equations XI and XII the concentration of free and bound ANS can be calculated for each sample.

Figure 88 shows a plot of bound ANS as a function of free ANS for all the compositions assayed. From these images it can be clearly seen that pure CL and pure POPE show the maximum and minimum decrease due to *cyt c* adsorption.

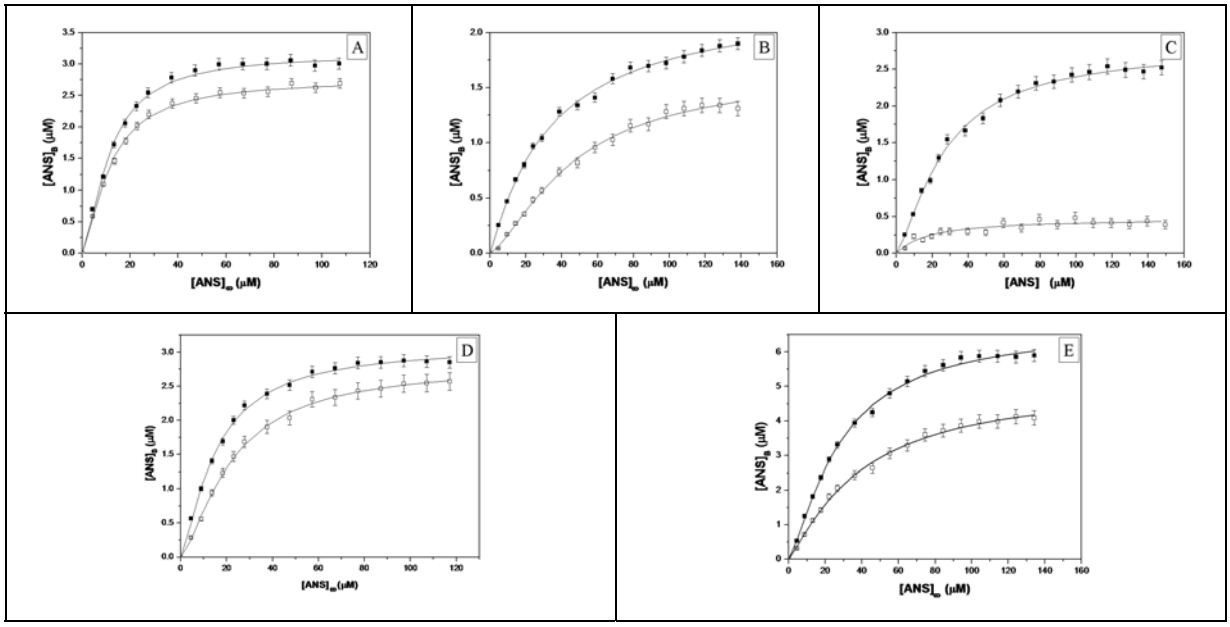

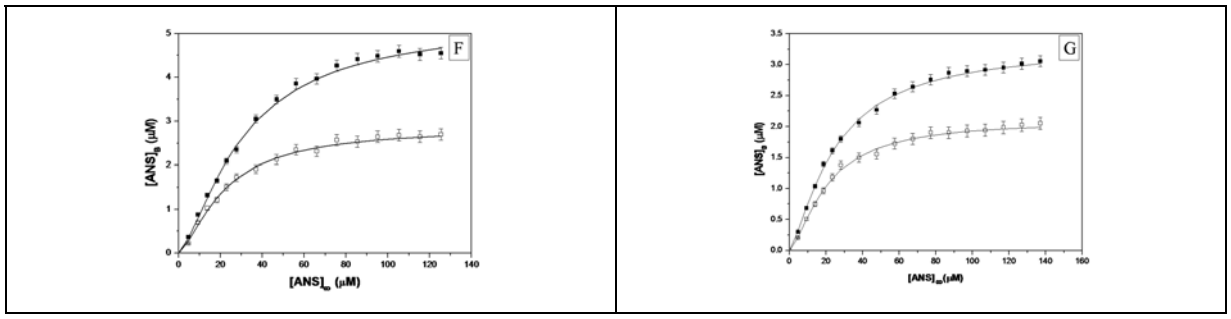

Figure 88. Bound ANS concentration as a function of free ANS concentration for samples with (□) and without (■) *cyt c* for A) POPC, B) POPE, C) CL, D) POPE:POPC (0.6:0.4, mol:mol), E) POPC:CL (0.6:0.4, mol:mol), F) POPE:CL (0.8:0.2, mol:mol) and G) POPE:POPC:CL (0.5:0.3:0.2, mol:mol:mol).

Table XV shows the parameters used to fit data from samples without *cyt c* to equation XIII, where the number of binding sites (*n*) was taken as one.

Table XV. Parameters from equation XIII for samples without *cyt c* and with a value of *n* of 1.

Lipid composition	C_0 (μM)	k_0 (μM^{-1})	b_0
POPC	4.11 ± 0.05	0.073 ± 0.002	1.35 ± 0.04
POPE	3.7 ± 0.2	0.017 ± 0.002	1.07 ± 0.07
CL	2.92 ± 0.13	0.034 ± 0.003	1.3 ± 0.2
POPE:POPC (0.6:0.4, mol:mol)	3.21 ± 0.07	0.062 ± 0.003	1.28 ± 0.06
POPC:CL (0.6:0.4, mol:mol)	7.4 ± 0.2	0.0306 ± 0.0018	1.22 ± 0.05
POPE:CL (0.8:0.2, mol:mol)	6.4 ± 0.4	0.023 ± 0.003	1.21 ± 0.09
POPE:POPC:CL (0.5:0.3:0.2, mol:mol:mol)	3.39 ± 0.07	0.0388 ± 0.0016	1.31 ± 0.05

From this table it can be seen that the POPC sample shows the highest association constant and the highest cooperativity values. By contrast, the POPE sample shows the lowest association constant and cooperativity values. Error values in all cases are below 15 % of the corresponding absolute value.

Table XVI shows the parameters used to fit data from samples with *cyt c* to equation XIII, where the value of *n* was taken as two.

Table XVI. Parameters from equation XIII for samples with *cyt c* and with a value of *n* of 2.

Lipid composition	C_1 (μM)	C_2 (μM)	k_1 (μM^{-1})	k_2 (μM^{-1})	b_1	b_2
POPC	3.22 ± 0.12	0.18 ± 0.10	0.098 ± 0.004	0.055 ± 0.004	1.48 ± 0.06	11 ± 12
POPE	2.3 ± 0.3	0.31 ± 0.16	0.034 ± 0.008	0.012 ± 0.005	1.21 ± 0.12	8 ± 4
CL	0.38 ± 0.02	0.061 ± 0.011	0.067 ± 0.005	0.0121 ± 0.0004	1.37 ± 0.08	11 ± 4
POPE:POPC (0.6:0.4, mol:mol)	2.4 ± 0.3	0.3 ± 0.2	0.052 ± 0.004	0.044 ± 0.005	1.41 ± 0.17	6 ± 5
POPC:CL (0.6:0.4, mol:mol)	3.5 ± 0.5	0.9 ± 0.4	0.045 ± 0.009	0.014 ± 0.006	1.52 ± 0.16	5 ± 2
POPE:CL (0.8:0.2, mol:mol)	1.7 ± 0.2	0.7 ± 0.2	0.055 ± 0.011	0.023 ± 0.009	1.8 ± 0.2	8 ± 3
POPE:POPC:CL (0.5:0.3:0.2, mol:mol:mol)	1.95 ± 0.16	0.21 ± 0.12	0.065 ± 0.008	0.0172 ± 0.0013	1.55 ± 0.15	8 ± 6

From Table XVI it can be clearly seen that the second binding site shows lower values of C_i and k_i and higher values of b_i than the first binding site. Also, the error values of C_i and b_i for the second binding site are much higher than those for the first binding site. However, the best fit to equation XIII is provided by the data with a second binding site.

From this table, as in the case of samples without *cyt c*, POPC and POPE show the highest and lowest association constant values, respectively. In this case, the cooperativity values are very similar for all samples and the differences are within the error values. Interestingly, pure CL shows the lowest C_i values, which indicates that few ANS molecules are bound to the liposome because of the large number of *cyt c* molecules occupying the possible binding sites.

Values of $\Delta\Psi$ can be calculated from the values of k_i in Tables XV and XVI and with equation XIII. Table XVII summarizes the values of $\Delta\Psi$ due to *cyt c* incorporation for all samples assayed.

Table XVII. $\Delta\Psi$ values due to *cyt c* incorporation.

Lipid composition	$\Delta\Psi$(mV)
POPC	+ 1.2 ± 0.2
POPE	+ 7.5 ± 0.4
CL	+ 13.4 ± 1.5
POPE:POPC (0.6:0.4, mol:mol)	- 6.5 ± 0.7
POPC:CL (0.6:0.4, mol:mol)	- 0.9 ± 0.4
POPE:CL (0.8:0.2, mol:mol)	+ 13.5 ± 0.6
POPE:POPC:CL (0.5:0.3:0.2, mol:mol:mol)	+ 1.5 ± 0.3

From this table it can be seen that the maximum increase in surface electrostatic potential due to *cyt c* incorporation is shown by pure CL and POPE:CL (0.8:0.2, mol:mol) with a mean value of + 13.5 mV. By contrast, the surface electrostatic potential of the POPE:POPC mixture (0.6:0.4, mol:mol) decreases, its absolute value being 6.5 mV. POPC, POPC:CL (0.6:0.4, mol:mol) and POPE:POPC:CL (0.5:0.3:0.2, mol:mol:mol) samples show a variation in the absolute value of surface electrostatic potential of ~ 1 mV, while the $\Delta\Psi$ value of the POPE sample shows an increase of + 7.5 mV.

V.3.4. Effect of surface charge in liposomes

In previous sections there is evidence that *cyt c* binds preferentially with samples containing CL. In order to determine whether this effect is due to charge or to a specific binding of *cyt c* to CL molecules, a new experiment was performed. In this experiment CL molecules were replaced by POPG molecules, but since CL is a double phospholipid the molar fraction of POPG in the samples was doubled.

Figure 89 shows the variation in fluorescence emission of POPC:POPG (0.43:0.57, mol:mol) and POPE:CL (0.66:0.33, mol:mol) as a function of ANS concentration in the cuvette.

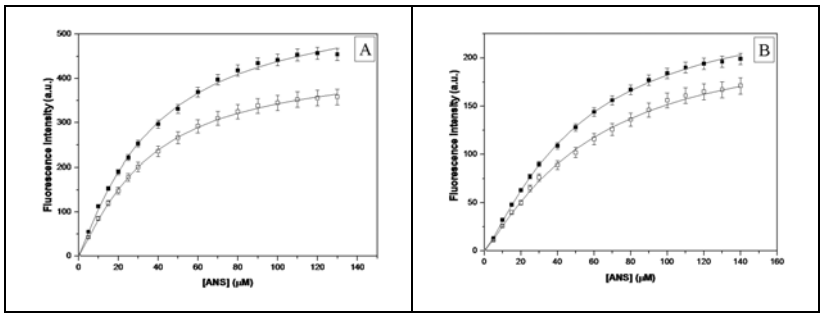

Figure 89. Fluorescence intensity variation as a function of ANS concentration for samples with (□) and without (■) *cyt c* for A) POPC:POPG(0.47:0.53, mol:mol), B) POPE:POPG(0.66:0.33, mol:mol).

As in previous sections, the sample containing POPC shows higher fluorescence emission than the sample containing POPE. In both samples, as expected, *cyt c* adsorption causes a decrease in the emission fluorescence.

The concentrations of free and bound ANS were calculated as in section V.3.1.2. Figure 90 shows the variation in bound ANS as a function of free ANS for both lipid mixtures.

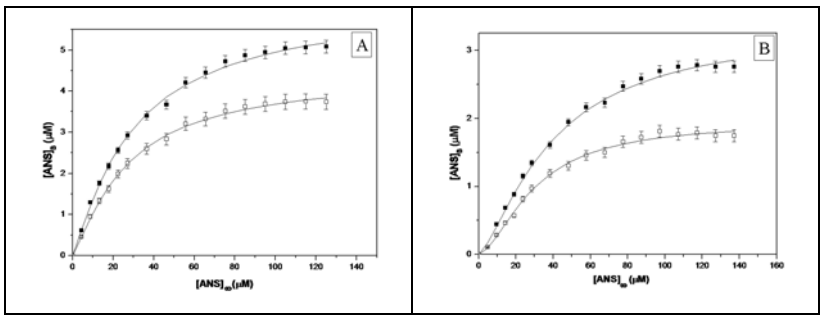

Figure 90. Bound ANS concentration as a function of free ANS concentration for samples with (□) and without (■) *cyt c* for A) POPC:POPG(0.47:0.53, mol:mol) and B) POPE:POPG(0.66:0.33, mol:mol).

From this image it is clearly seen that *cyt c* shows similar adsorption in both compositions despite the fact that the POPG concentration in POPC:POPG is higher than in POPE:POPG liposomes.

Table XVIII shows the parameters that fit the data from samples without *cyt c* to equation XIII, where the value of binding sites (n) was taken as one. Liposomes containing POPC show higher values of C_0 and k_0 than liposomes containing POPE. The value of b_0 is similar in both cases.

Table XVIII. Parameters from equation XIII for samples without *cyt c* and with a value of *n* of 1.

Lipid composition	C_0 (μM)	k_0 (μM^{-1})	b_0
POPC:POPG (0.43:0.57, mol:mol)	6.3 ± 0.2	0.032 ± 0.002	1.12 ± 0.06
POPE:POPG (0.66:0.33, mol:mol)	3.27 ± 0.09	0.0271 ± 0.0014	1.46 ± 0.07

Table XIX shows the parameters that fit the data from samples with *cyt c* to equation XIII, where the value of *n* was taken as two.

Table XIX. Parameters from equation XIII for samples with *cyt c* and with a value of *n* of 2.

Lipid composition	C_1 (μM)	C_2 (μM)	k_1 (μM^{-1})	k_2 (μM^{-1})	b_1	b_2
POPC:POPG (0.43:0.57, mol:mol)	3.2 ± 1.2	0.8 ± 0.7	0.06 ± 0.03	0.0195 ± 0.0017	1.4 ± 0.3	4 ± 2
POPE:POPG (0.66:0.33, mol:mol)	1.74 ± 0.12	0.13 ± 0.08	0.0387 ± 0.004	0.0234 ± 0.0013	1.85 ± 0.18	2 ± 4

In this case too, the sample containing POPC incubated with *cyt c* shows higher values of C_i and k_i than the sample containing POPE. The values of b_i are quite similar in both cases.

As in the previous section, the values of $\Delta\Psi$ are calculated from the values of k_i in Tables XVII and XVIII and with equation XIII. Table XX summarizes the values of $\Delta\Psi$ due to *cyt c* incorporation for both samples.

Table XX. $\Delta\Psi$ values due to *cyt c* incorporation.

Lipid composition	$\Delta\Psi$ (mV)
POPC:POPG (0.43:0.57, mol:mol)	+ 5.6
POPE:POPG (0.66:0.33, mol:mol)	+ 3.5

From Table XIX it can be clearly seen that the POPC:POPG (0.43:0.57, mol:mol) sample shows a higher value of $\Delta\Psi$ than the POPE:POPG (0.66:0.33, mol:mol) sample. This result can be expected if it is taken into account that the molar concentration of POPG is greater in the POPC sample than in the POPE sample. As a result, *cyt c* binds similarly to both samples but the $\Delta\Psi$ value in POPC:POPG (0.43:0.57, mol:mol) is higher as more POPG molecules are present in its composition.

V.4. AFM SPB CHARACTERIZATION

SPBs of desired compositions were prepared as described in section IV.1.5.

V.4.1. SPB of POPE:POPC (0.6:0.4, mol:mol)

Figure 91 shows three sequences of topographic, amplitude and phase AFM images at temperatures of 4 ºC (A, B and C), 24 ºC (D, E and F) and 37 ºC (G, H and I).

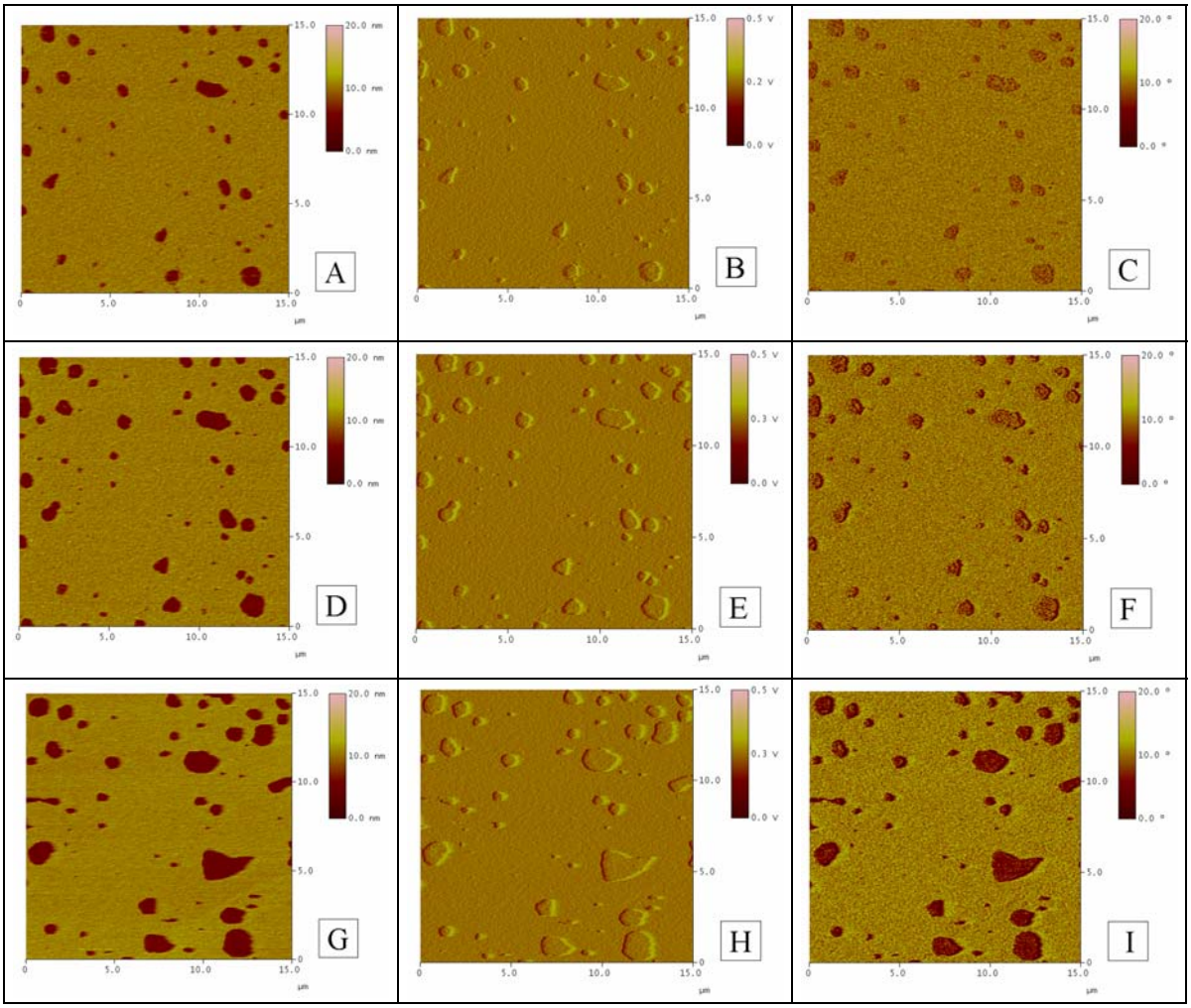

Figure 91. Topographic, amplitude and phase AFM images of POPE:POPC (0.6:0.4, mol:mol) SPB at 4 ºC (A, B, C), 24 ºC (D, E, F) and 37 ºC (G, H, I).

From the topographic images (A, D and G) it can be seen that SPB covers almost the entire mica surface (bright region) but several defects reveal the mica surface (dark region). The defects have been used to infer the depth of these SPBs, which are determined as 5.90 nm, 5.70 nm and 5.20 nm at 4 ºC, 24 ºC and 37 ºC, respectively. The

SPB mean roughness values at 4 ºC and 24 ºC are very similar (*Ra* ~ 0.45 nm) while at 37 ºC the SPB is smoother (*Ra* ~ 0.38 nm). It is well known that at high temperatures, the molecules in the bilayer have greater mobility than at low temperatures because of the increase in the diffusion coefficient. This effect decreases the roughness observed. The holes in topographic images are smaller in diameter at 4 ºC than at 37 ºC as can be seen if we consider that the percentage of the mica surface covered by the SPB is 93 % at 4 ºC and falls to 88 % at 37 ºC.

From the amplitude images (B, E and H) it can be seen that the mica and SPB surfaces are flat and do not show any accumulated material.

In the phase images (C, F and I) the two surfaces are easily distinguishable from one other. The mica surface is darker than the SPB surface and this colour contrast is more pronounced at 37 ºC than at 4 ºC. This indicates that at 37 ºC the viscoelastic properties between the mica surface and SPB surface are more marked than at 4 ºC.

Table XXI summarizes the topographic parameters of POPE:POPC (0.6:0.4, mol:mol) SPB from Figure 91.

Table XXI. Parameters of the POPE:POPC (0.6:0.4, mol:mol) SPB at different temperatures.

Temperature	h (nm)	*Ra* (nm)	Covering (%)
4 ºC	5.9 ± 0.3	0.45	93
24 ºC	5.7 ± 0.3	0.44	91
37 ºC	5.2 ± 0.2	0.38	88

V.4.2. SPB of POPC:CL (0.6:0.4, mol:mol)

Figure 92 shows three sequences of topographic, amplitude and phase AFM images at temperatures of 4 ºC (A, B and C), 24 ºC (D, E and F) and 37 ºC (G, H and I).

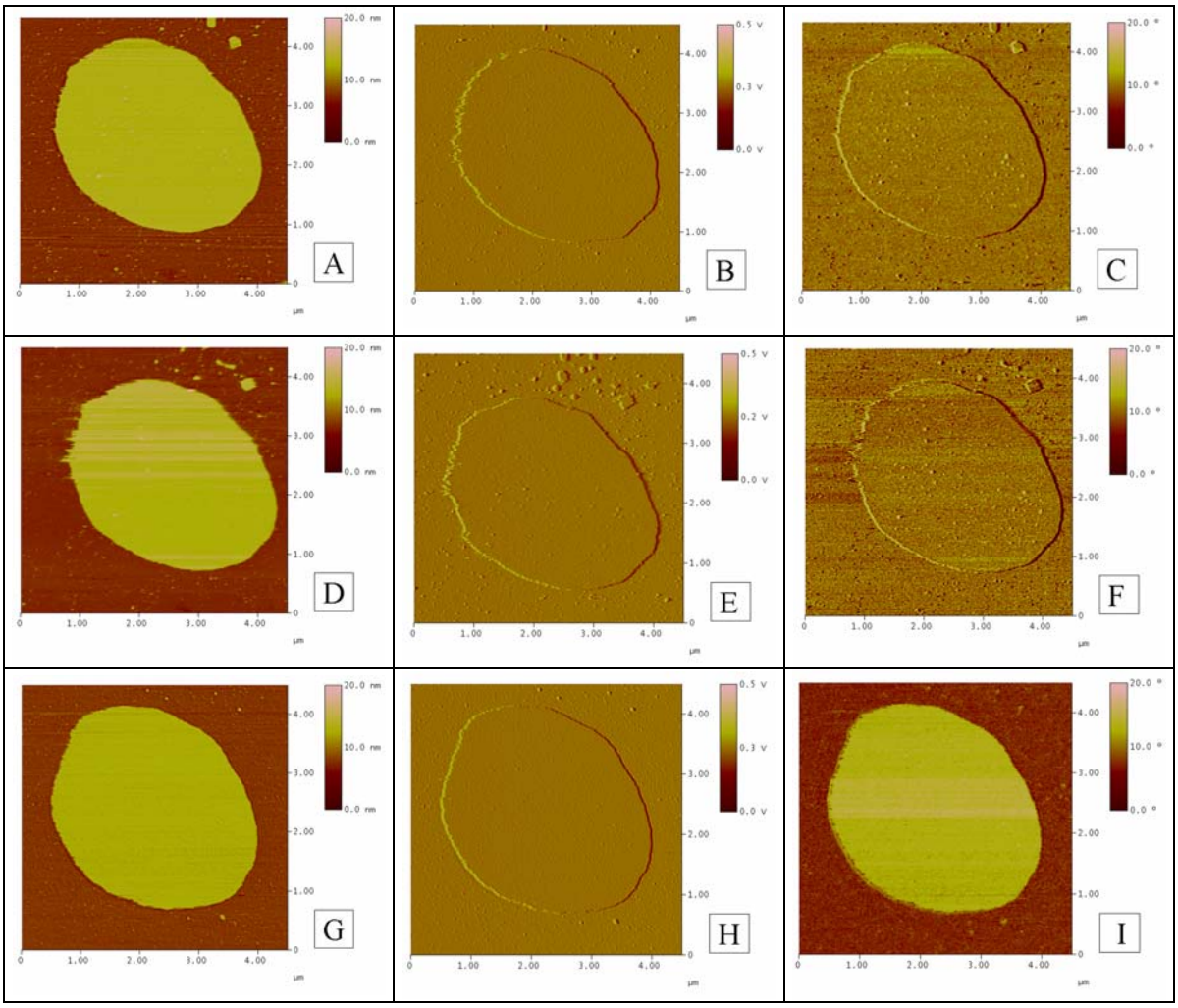

Figure 92. Topographic, amplitude and phase AFM images of POPC:CL (0.6:0.4, mol:mol) SPB at 4 ºC (A, B, C), 24 ºC (D, E, F) and 37 ºC (G, H, I).

From the topographic images (A, D and G) it can be seen that POPC:CL (0.6:0.4, mol:mol) SPBs do not form large bilayer extensions. The dark region in the images is the mica surface, while the bright yellow structure is the SPB surface. The extension of liposomes of this composition generally forms flat, round structures with diameters from 3 to 5 μm and a large number of small, circular structures with diameters of ~ 200 nm close to them. These small lipid structures can be interpreted as small SPBs that coalesce to form larger SPBs. There is probably not sufficient incubation time for the complete integration into the largest SPB. The SPB at 24 ºC (image D) shows several deformations on its surface caused by scratching the SPB with the AFM tip. Interestingly, at 37 ºC (image G) the small circular structures on the top-right edge observed in the other two images are not visible. This could be caused either by the desorption of molecules at higher temperatures towards the solution or by the incorporation of molecules into the SPB. The step height differences between SPB and

mica at different temperatures were determined using section analysis profiles with mean height values of 5.60 nm, 4.52 nm and 4.4 nm at 4 ºC, 24 ºC and 37 ºC, respectively. Interestingly, the absolute values of *Ra* increase with temperature from ~ 0.15 nm at 4 ºC to ~ 0.30 nm at 37 ºC. The increase of *Ra* at higher temperatures could be caused by the tip, which can easily deform the SPB, thus pulling molecules up.

From the amplitude images (B, E and H) it can be seen that at temperatures below 25 ºC protrusions are visible on the SPB surface. These protrusions are spherical in shape, have a mean diameter of ~ 50 nm and are distributed on the surface as well as the mica substrate. In image H, where the visualization temperature is 37 ºC, these round structures do not appear on the SPB surface and only large structures appear on the mica surface. These protrusions could be caused by the aggregation of lipids on the SPB surface that at 37 ºC are integrated into the SPB, due to the increase of its molecular mobility.

In phase images at 4 ºC and 24 ºC (images C and F) there are no appreciable differences in phase between the mica surface and SPB surface. In image C protrusions can be seen on the SPB whereas in image B they do not appear; these protrusions are also clearly visible in images E and F. In the phase image at 37 ºC (image I) the mica surface and SPB surface can be distinguished because of the colour contrast: the mica surface is the dark red region while SPB is the round yellow structure. This suggests that SPB displays different viscoelastic properties at 37 ºC than at 24 ºC or 4 ºC.

Table XXII summarizes the topographic parameters of POPC:CL (0.6:0.4, mol:mol) SPB from Figure 92.

Table XXII. Parameters of the POPC:CL (0.6:0.4, mol:mol) SPB at different temperatures.

Temperature	h (nm)	*Ra* (nm)
4 ºC	5.60 ± 0.18	0.15
24 ºC	4.52 ± 0.16	0.18
37 ºC	4.4 ± 0.3	0.30

V.3.3. SPB of POPE:CL (0.8:0.2, mol:mol)

Figure 93 shows an AFM image of an SPB of liposomes of POPE:CL (0.8:0.2, mol:mol) at 24 ºC.

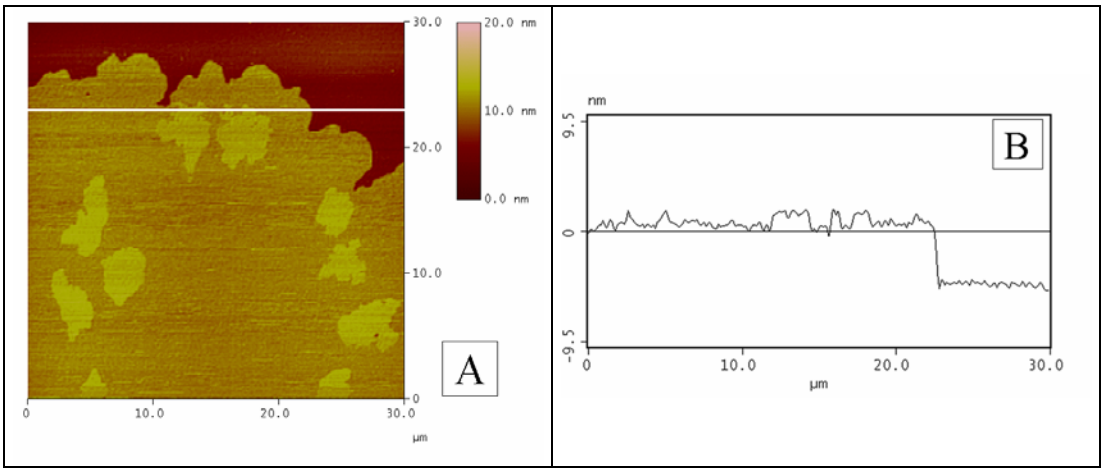

Figure 93. (A) AFM topographic image of an SPB of POPE:CL (0.8:0.2, mol:mol). (B) Height profile analysis along white line drawn in Figure 93A.

Image 93A shows a large SPB on the mica surface where the lateral segregation of lipids is revealed by differences in the colour scale. In this image the low lipid domain has a mean height over the mica (darkest region in the image) of 5.1 nm with an *Ra* value of 0.16 nm. The high lipid domain has a mean height over the low domain of 1.5 nm and an *Ra* value of 0.13 nm. This high lipid domain represents 17 % of the total surface of the extended SPB. Interestingly, this percentage is quite similar to the CL molar fraction in SPB composition. Figure 93B is a topographic profile through the different regions of the SPB that shows the heights of the lipid domains.

Figure 94 shows a sequence of images of the SPB in Figure 93 as the sample temperature increases from 4 ºC (images A and D) to 37 ºC (images C and F). From the topographic image at 4 ºC (image A) two lipid domains can be identified in the SPB. From the corresponding amplitude image at 4 ºC (image D) it can be seen that both lipid domains are flat. When the temperature is increased to 24 ºC a new lipid domain can be observed in the topographic image (image B). Initially it can be seen as small round structures, 0.45 nm lower than the low domain from image A (black arrows in images B and C) indicated with white arrows in image B. At this point, three lipid domains coexist: low, intermediate and high. From the amplitude image of B (image E) it can be

seen that the low domain, now composed of two lipid domains, is rougher when the temperature is increased.

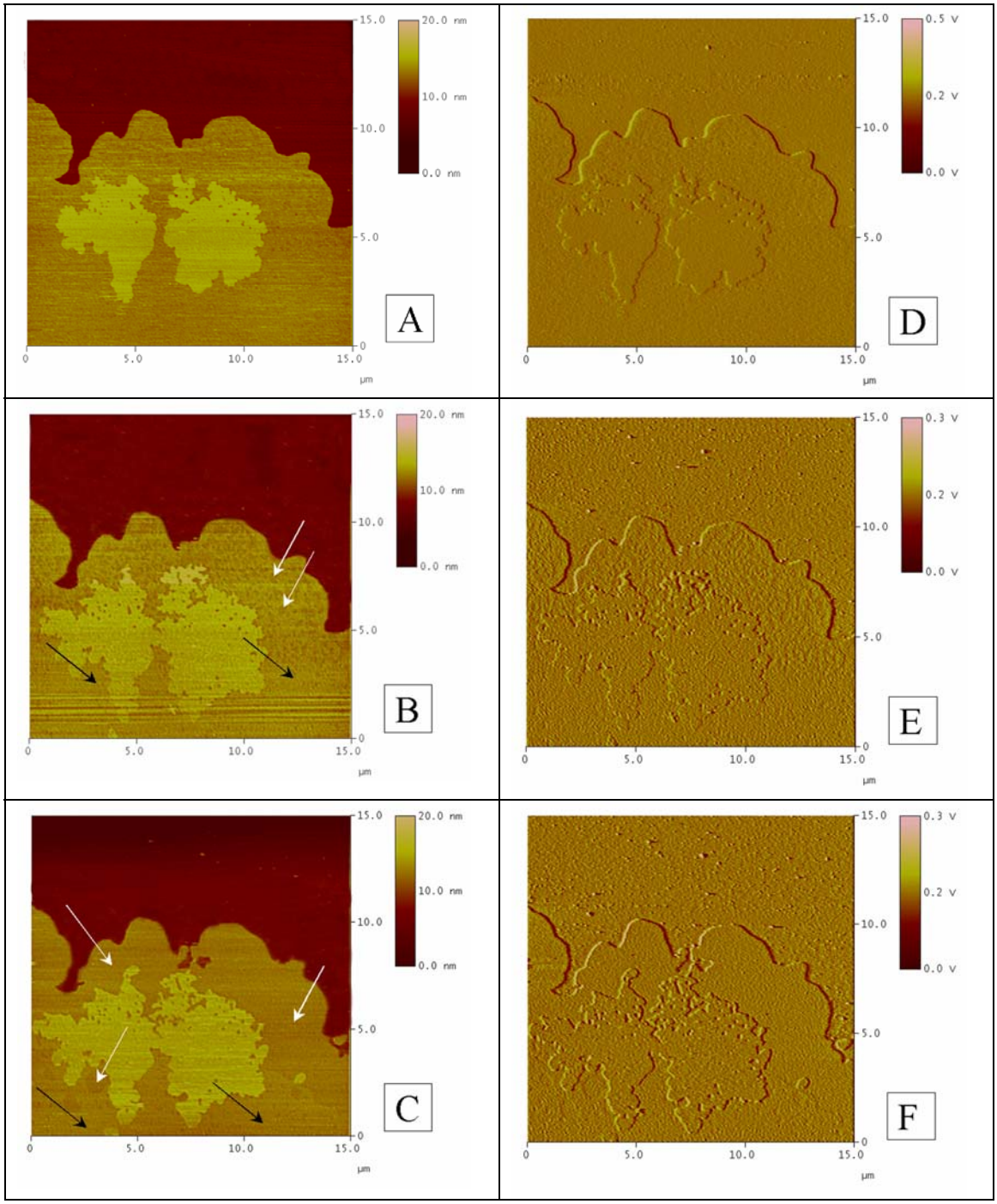

Figure 94. More resolution AFM topographic and amplitude images of the same SPB presented in Figure 93 during the increase of sample temperature from A) 4 ºC to C) 37 ºC. White and black arrows correspond to low and high domains.

In image C the sample is shown at 37 ºC and the new lipid domain that appears in image B (white arrows) is extended over a large area, restricting intermediate domain (black arrows) to a smaller area. From the corresponding amplitude image (image F) it can be seen that the low lipid domain is flatter than the intermediate domain.

Table XXIII summarizes the topographic parameters of POPE:CL (0.8:0.2, mol:mol) SPB.

Table XXIII. Parameters of POPE:CL (0.8:0.2, mol:mol) SPB at different temperatures.

Temperature	Domain height (nm)			Domain *Ra* (nm)		
	Low	**Intermediate**	**High**	**Low**	**Intermediate**	**High**
4 ºC	4.8 ± 0.3	-	6.8 ± 0.2	0.11	-	0.10
24 ºC	4.7 ± 0.2	5.1 ± 0.2	6.6 ± 0.2	0.14	0.16	0.13
37 ºC	4.2 ± 0.2	4.70 ± 0.10	6.4 ± 0.2	0.17	0.19	0.23

To investigate the nature of the different lipid domains new experiments were performed with the same lipid composition. Figure 95 shows four topographic AFM images at different temperatures. Figure 95A shows an SPB of POPE:CL (0.8:0.2, mol:mol) at 24 ºC in which two lipid domains are present: the upper and the intermediate domains. When the temperature is increased to 37 ºC a new phospholipid domain appears at the expense of the intermediate domain (Figure 95B) and increases its surface area in successive scans at this temperature (Figures 95C and 95D). Although the upper domain is unchanged between Figures 95A and 95B, its surface area is larger in Figure 95C.

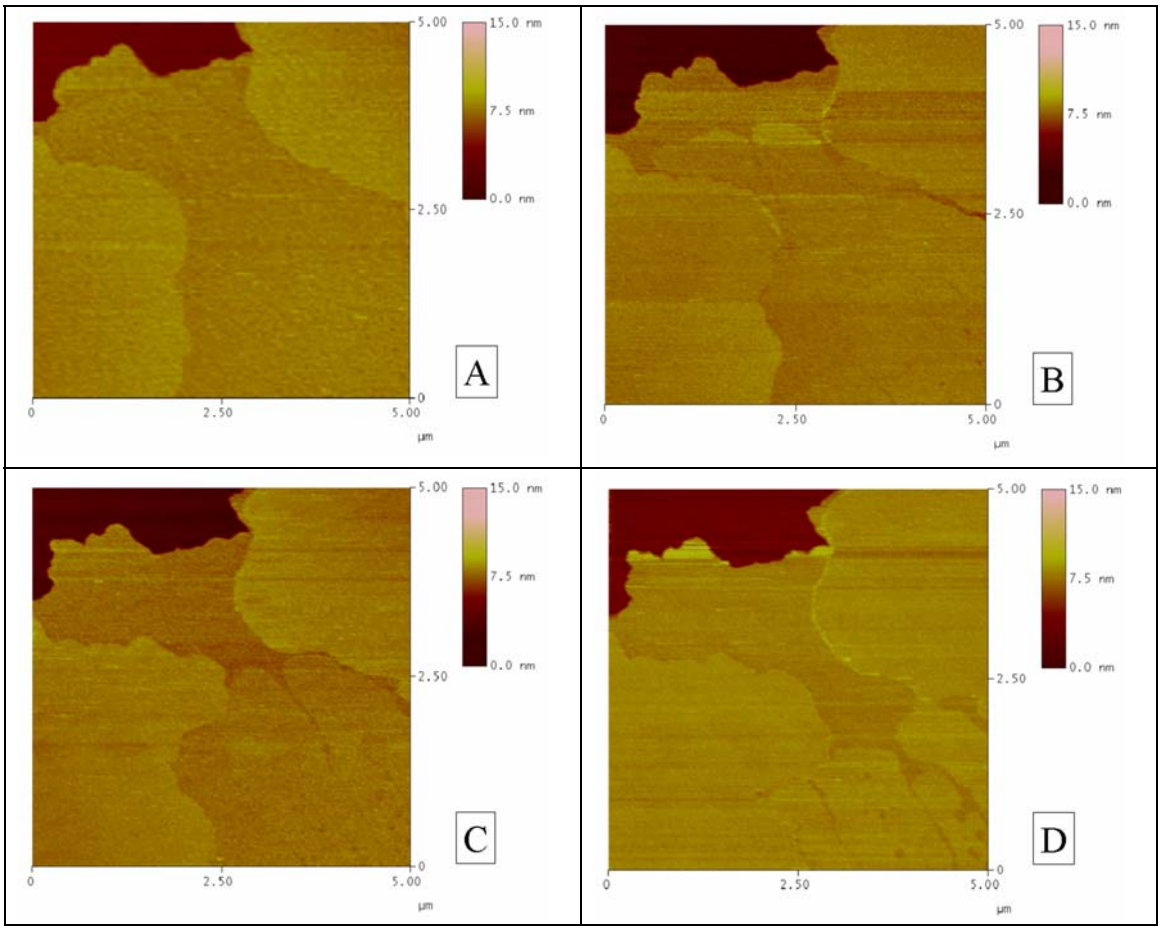

Figure 95. Sequence of AFM topographic images of POPE:CL (0.8:0.2, mol:mol) SPB before and after increasing the sample temperature. Figure 95A shows the SPB at 24 ºC in which only two lipid domains can be seen. In Figure 95B the temperature is increased to 37 ºC and a new lipid domain appears and increases its surface area (Figure 95C and 95D).

Figure 96 shows two AFM images of an SPB of POPE:CL (0.8:0.2, mol:mol) composition. The figure contains topographic (A and C) and deflection (B and D) images in which two lipid domains can be easily distinguished at 24 ºC.

From image 96A we can infer the bilayer thickness measuring the step height between the top of the layer and the uncovered mica (red colour in the lower-left corner). Thus, while the height of the lower domain (4.64 nm) falls within the range expected for bilayer thickness, the upper domain appears as an upper layer, with a height of ~ 1.00 nm above the lower domain. Accordingly, the thickness of the upper layer is consistent with the depth of numerous defects (holes) observed.

As the high lipid domain is present at all temperatures, it was repeatedly scanned in contact mode at a force of ~ 30 nN for 20 seconds (image 96C and 96D) to provide a more detailed analysis. The upper layer on the SPB surface becomes unstable and the lipid molecules can be swept away, which deforms the shape of the lipid domain.

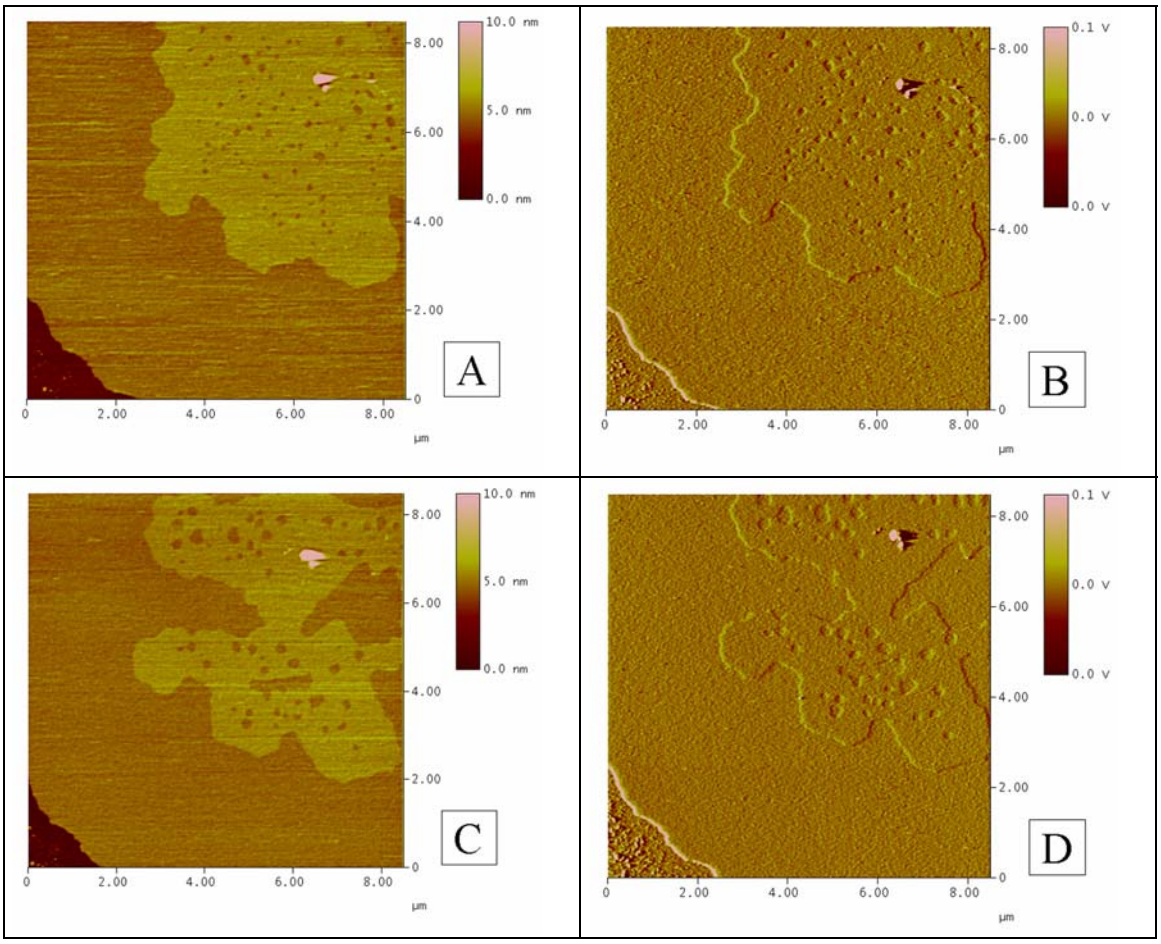

Figure 96. AFM topographic (A and B) and deflection (C and D) images of a POPE:CL (0.8:0.2, mol:mol) SPB before (images A and B) and after (images C and D) the surface was scratched with the AFM tip.

Figure 97 shows two section analyses from the topographic images in Figure 96.

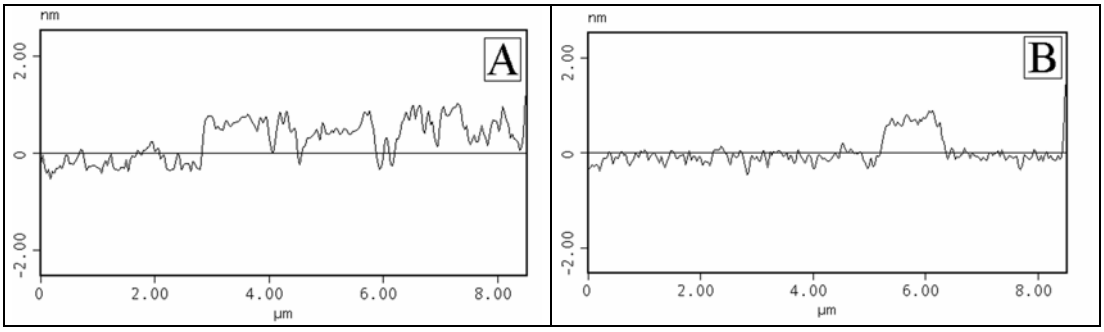

Figure 97. Section analysis from topographic images in Figure 96 A) before and B) after scratching the surface of the SPB.

Figures 97A and 97B are the height profiles before and after the deformation of the SPB surface, respectively. This observation is consistent with the fact that the surface covering the lower domain decreases. Furthermore, the height of the upper domain is confirmed by measuring the depth of the scratched area. As expected, the resulting measurement (~ 0.94 nm) coincides with the inter-domain height reported above.

V.3.3.1. DSC and NMR analysis of POPE:CL (0.8:0.2, mol:mol) samples

Lipid domains appeared in all of the above images when the temperature was increased. Therefore, the thermal response of these samples was investigated using DSC.

Figure 98 shows the endotherm of POPE:CL (0.8:0.2, mol:mol) samples resuspended in 20 mM Hepes, 150 mM NaCl, at pH 7.40 (dashed line) and 20 mM Hepes, 150 mM NaCl, 20 mM $CaCl_2$ at pH 7.40 (continuous line).

Calcium-free endotherms (dashed line) show a wide transition centred at 15.6 ºC, while in the presence of calcium (continuous line) the main transition occurs at 20.9 ºC and is wider than at 15.6 ºC. This second endotherm is similar to the endotherm of the pure phospholipid.

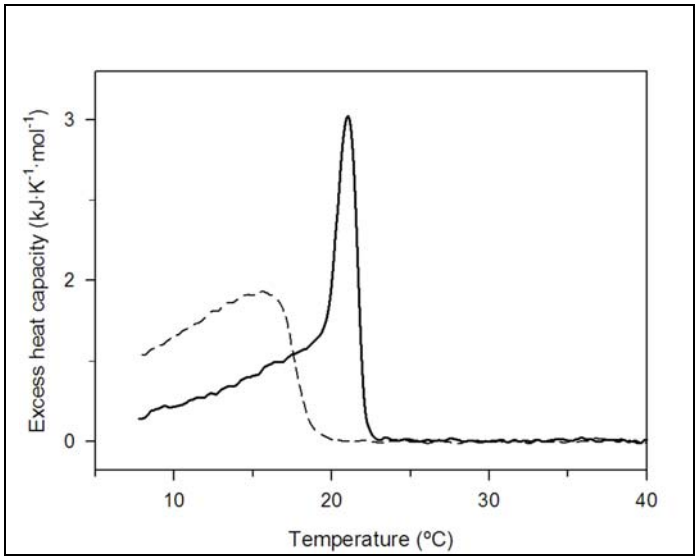

Figure 98. DSC endotherm of POPE:CL (0.8:0.2, mol:mol) samples. Continuous and dashed lines represent samples with and without calcium in the resuspension buffer.

Figure 99 shows solid state ^{31}P-NMR spectra of POPE:CL (0.8:0.2, mol:mol) samples at different temperatures. The spectra show different shapes in the presence or absence of calcium in the aqueous media. The sample without calcium (dashed lines) is mainly composed of vesicles while when calcium is present in the resuspension buffer (continuous lines) two structures, vesicles and hexagonal phases (H_{II}) can be seen. Interestingly, at 15 ºC the sample containing calcium shows a hump at positive chemical shifts, which indicates that vesicles are present in the sample at this temperature. At higher temperatures this hump is reduced and hexagonal phases become the predominant phase in solution.

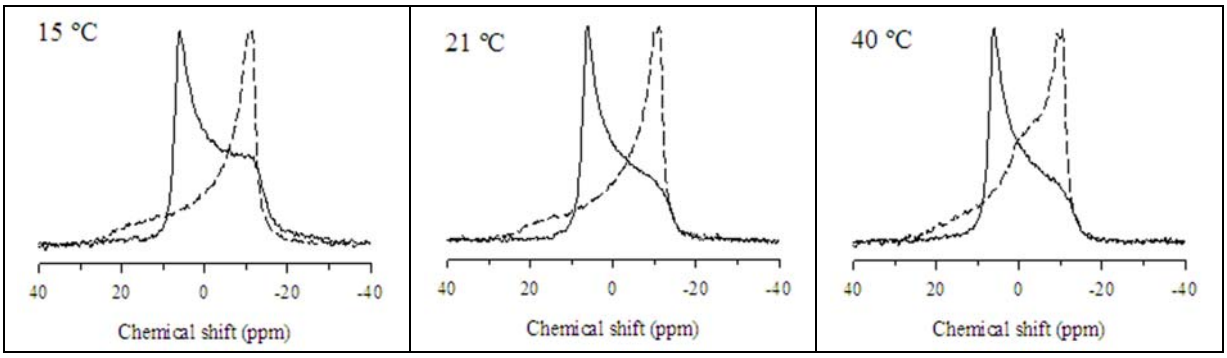

Figure 99. Solid state 31P-NMR spectra of POPE:CL (0.8:0.2, mol/mol) dispersions at 15 ºC, 21 ºC and 40 ºC. Continuous and dashed lines show samples with and without calcium in the resuspension buffer.

V.3.4. SPB of POPE:POPC:CL (0.5:0.3:0.2, mol:mol:mol)

Figure 100 shows three sequences of topographic, amplitude and phase AFM images at temperatures of 4 ºC (A, B and C), 24 ºC (D, E and F) and 37 ºC (G, H and I).

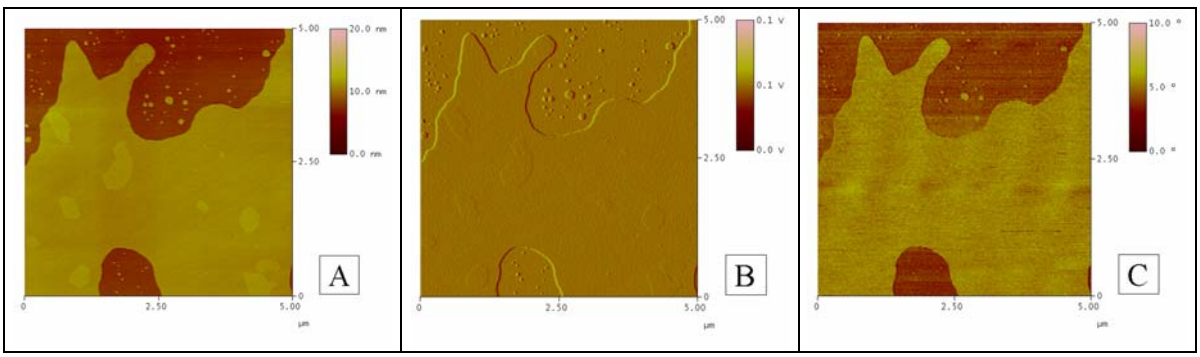

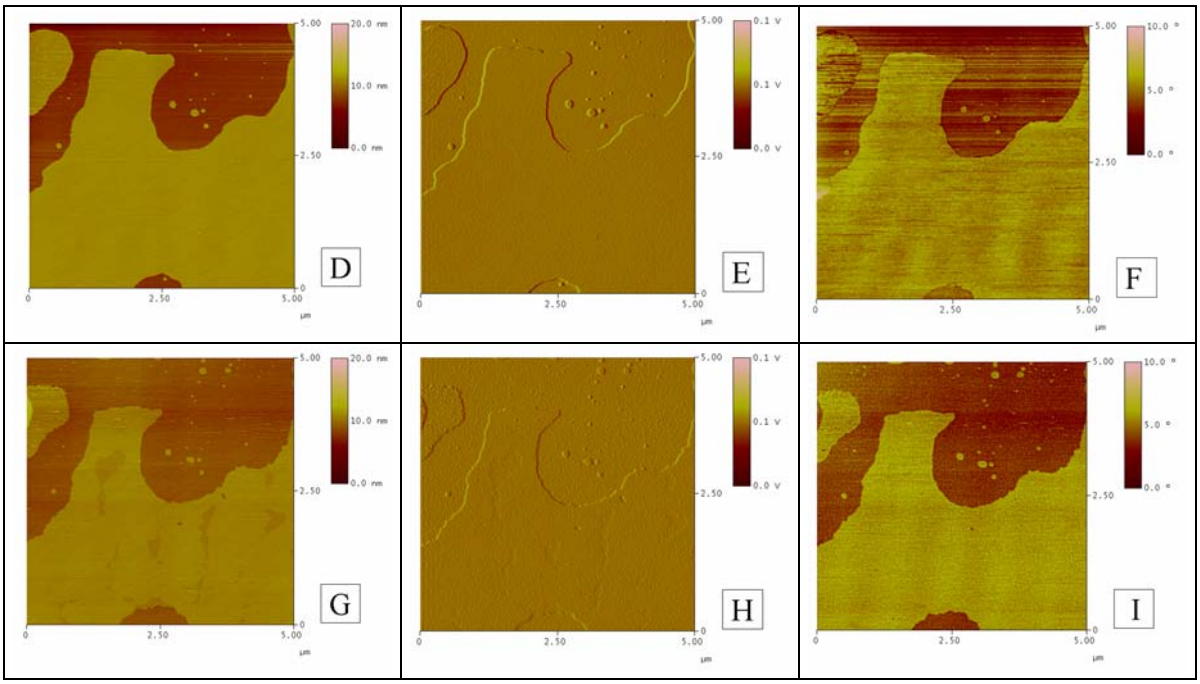

Figure 100. AFM topographic, amplitude and phase images of POPE:POPC:CL (0.5:0.3:0.2, mol:mol:mol) SPB at 4 ºC (A, B, C), 24 ºC (D, E, F) and 37 ºC (G, H, I).

The topographic images (A, D and G) show SPB extensions with several small round structures close by. In these images the mica surface is the dark red region while structures of different shades of yellow can be seen on the SPB surface. In image A, at 4 ºC, the SPB is composed of two different lipid domains. The high lipid domain has a height of 4.1 nm with an *Ra* value of 0.13 nm and the low lipid domain has a height of 3.5 nm and an *Ra* value of 0.15 nm. In image D, at 24 ºC, only one lipid domain can be seen, which has a height of 3.5 nm and an *Ra* value of 0.14 nm. In image G, at 37 ºC, one new lipid domain appears on the SPB surface. At this temperature the SPB height is 2.4 nm with an *Ra* value of 0.14 nm, while the new lipid domain is 0.5 nm lower than the SPB surface with an *Ra* value of 0.10 nm. In summary, three different lipid domains appear at different temperatures: high, intermediate and low lipid domains. The intermediate lipid domain appears in all three images while the high and low lipid domains only appear at 4 ºC and 37 ºC, respectively. Interestingly, when the temperature is increased from 4 ºC to 24 ºC, the SPB surface is extended to a larger area. This effect can be appreciated due to the fusion of the two lipid appendixes at the top-left edge of image A.

In the amplitude images (B, E and H) the different lipid domains can be clearly distinguished. These domains and the mica surface are flat at all temperatures assayed and no structures can be seen on the SPB surface.

In the phase images (C, F and I) the mica surface and SPB surface are clearly distinguishable from one other due to the phase contrast. The mica surface always shows lower phase values than the SPB surface. In images at 4 ºC and 37 ºC (images C and I) the high and low lipid domains cannot be distinguished from the intermediate domain due to laser interference that produces wide vertical lines on the SPB surface.

Table XXIV summarizes the topographic parameters of the POPE:POPC:CL (0.5:0.3:0.2, mol:mol:mol) SPB from Figure 100.

Table XXIV. Parameters of the POPE:POPC:CL (0.5:0.3:0.2, mol:mol:mol) SPB at different temperatures.

Temperature	Domain height (nm)			Domain *Ra* (nm)		
	Low	Intermediate	High	Low	Intermediate	High
4 ºC	-	3.5 ± 0.3	4.1 ± 0.3	-	0.15	0.13
24 ºC	-	3.5 ± 0.2	-	-	0.14	-
37 ºC	1.9 ± 0.2	2.4 ± 0.2	-	0.10	0.14	-

V.5. *IN SITU CYT C* INCORPORATION INTO SPB

SPBs of desired compositions were prepared as described in section IV.1.5.

V.5.1 SPB of POPE:POPC (0.6:0.4, mol:mol)

Figure 101 shows two sequences of topographic, amplitude and phase AFM images before (A, B and C) and after (D, E and F) *cyt c* incorporation into the sample through the AFM liquid cell.

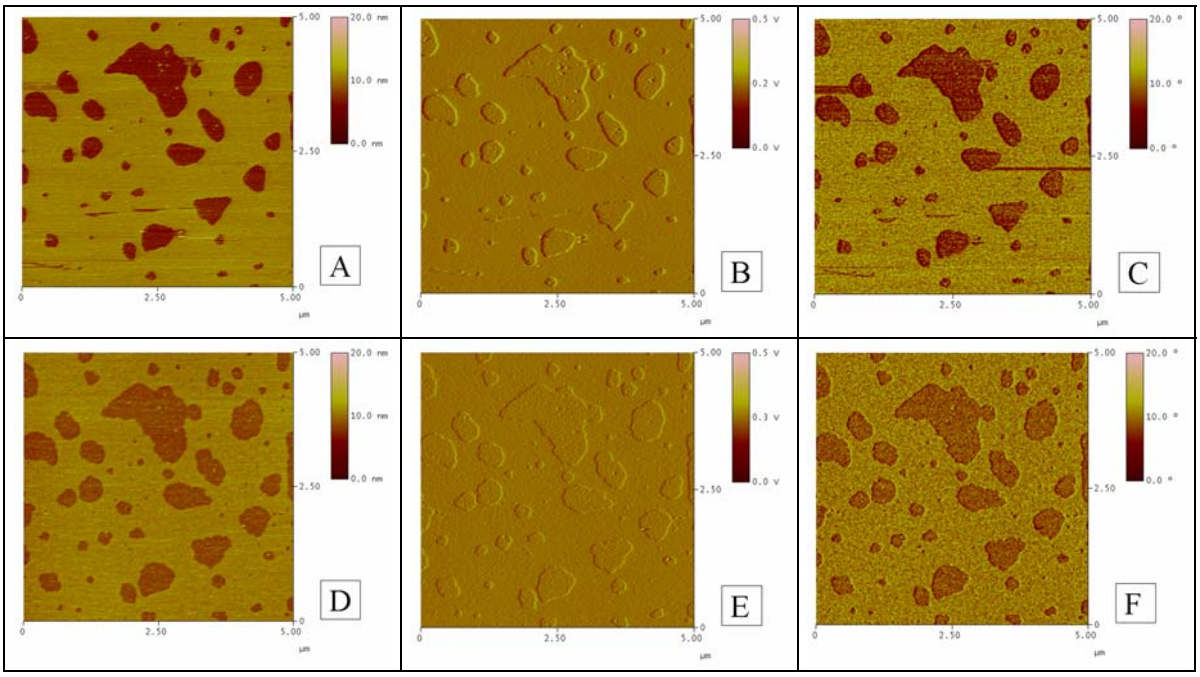

Figure 101. AFM topographic, amplitude and phase images of POPE:POPC (0.6:0.4, mol:mol) SPB before (A, B, C) and after (D, E, F) *cyt c* incorporation.

Image A shows that the SPB extension covers most of the substrate surface but leaves some uncovered mica regions. This SPB has a height of 5.70 nm and a mean *Ra* value of 0.27 nm. It can be seen from the uncovered mica that some sort of lipid aggregates are present on the mica surface, which have an *Ra* value of 0.38 nm. After *cyt c* incorporation (image D) the SPB has a height of 3.20 nm and an *Ra* value of 0.34 nm. Interestingly, the mica *Ra* value increases to 0.41 nm after *cyt c* incorporation. No adsorbed proteins are seen on the SPB, as reflected by the constant *Ra* value before and after *cyt c* injection, but the increase in the *Ra* value of the mica surface can be

considered the result of either *cyt c* deposition on the mica surface or the formation of lipid aggregates after *cyt c* injection.

The amplitude images (B and E) reveal material on the mica surface, particularly on large, uncovered regions. At the same scale, the image before *cyt c* incorporation shows a higher amplitude contrast between the mica surface and SPB surface than the image after *cyt c* incorporation.

In the phase images (C and F) the mica and SPB surfaces are easily distinguishable from one other before and after *cyt c* incorporation. Moreover, when *cyt c* is incorporated into the sample no new structures are visible in the phase image and the colour contrast between both surfaces is lower. This effect can be understood if *cyt c* proteins are adsorbed on only one of the two surfaces. If *cyt c* is only adsorbed on one of the surfaces, the phase contrast between surfaces can decrease.

Table XXV summarizes the topographic parameters of the POPE:POPC (0.6:0.4, mol:mol) SPB from Figure 101.

Table XXV. Parameters of the POPE:POPC (0.6:0.4, mol:mol) SPB before and after *cyt c* incorporation.

		***Cyt c* injection**	
		Before	**After**
h (nm)		5.70 ± 0.20	3.20 ± 0.30
***Ra* (nm)**	SPB	0.27	0.34
	Mica	0.38	0.41

V.5.2. SPB of POPC:CL (0.6:0.4, mol:mol)

Figure 102 shows two sequences of topographic, amplitude and phase AFM images before (A, B and C) and after (D, E and F) *cyt c* incorporation into the sample through the AFM liquid cell.

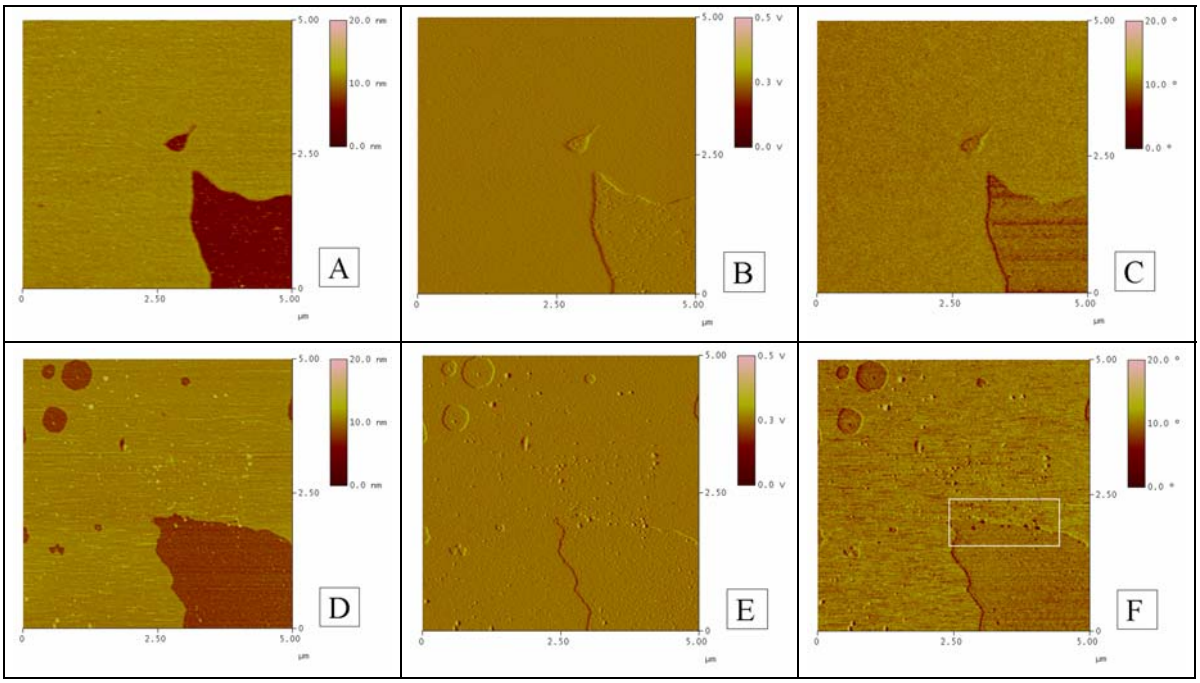

Figure 102. Topographic, amplitude and phase AFM images of POPC:CL (0.6:0.4, mol:mol) SPB before (A, B, C) and after (D, E, F) *cyt c* incorporation.

Image A (topographic image) shows an SPB of POPC:CL (0.6:0.4, mol:mol) in which the mica surface can be seen on the bottom-right edge as a dark red region. This SPB has a height of 4.50 nm and a mean *Ra* value of 0.31 nm. In this image mica shows an *Ra* value of 0.50 nm. After *cyt c* incorporation, the topographic image (image D) shows a large number of small structures (50 nm in diameter) on the SPB surface. Here, the SPB height is reduced to 2.80 nm with an *Ra* value of 0.37 nm. Furthermore, new uncovered mica appears after *cyt c* incorporation as round structures in the top left corner with a mean *Ra* value of 0.39 nm. The destruction of the SPB due to *cyt c* injection can be caused by different factors such as the difference in the local ionic strength, the lytic action of *cyt c* molecules on the SPB surface, among others.

In the amplitude image before *cyt c* incorporation (image B) the SPB is almost flat while the mica surface has a number of lipid structures on it. In the same image after *cyt c* incorporation (image E) small structures with diameters of 50 nm are clearly visible on the SPB surface.

Image C is the phase image of SPB before *cyt c* incorporation, in which the mica surface can be differentiated from the SPB surface by the colour scale. Image F shows the same region after *cyt c* incorporation, in which it can be seen that almost all of the

new protrusions that appear after protein injection have similar properties to the SPB surface. Interestingly, some of these structures close to the edge between the SPB and the mica surface have different properties to the SPB and mica surface. They can be identified as dark, round structures on the edge of the SPB enclosed by a white rectangle. The diameters of these structures, which show a different phase contrast to the SPB surface, suggest that they could be *cyt c* aggregates.

Table XXVI summarizes the topographic parameters of the POPC:CL (0.6:0.4, mol:mol) SPB from Figure 102.

Table XXVI. Parameters of the POPC:CL (0.6:0.4, mol:mol) SPB before and after *cyt c* incorporation.

		***Cyt c* injection**	
		Before	**After**
h (nm)		4.50 ± 0.20	2.80 ± 0.30
***Ra* (nm)**	SPB	0.31	0.37
	Mica	0.50	0.39

V.5.3. SPB of POPE:CL (0.8:0.2, mol:mol)

Figure 103 shows two sequences of topographic, amplitude and phase AFM images before (A, B and C) and after (D, E and F) *cyt c* incorporation into the sample into the AFM liquid cell.

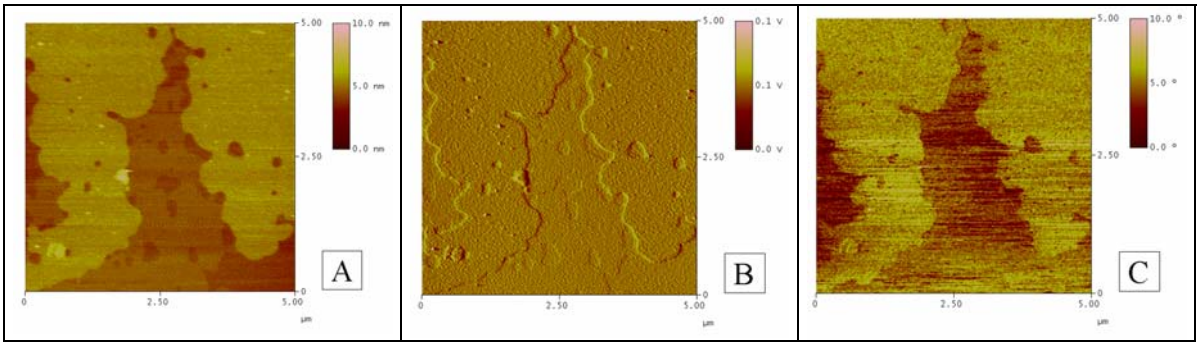

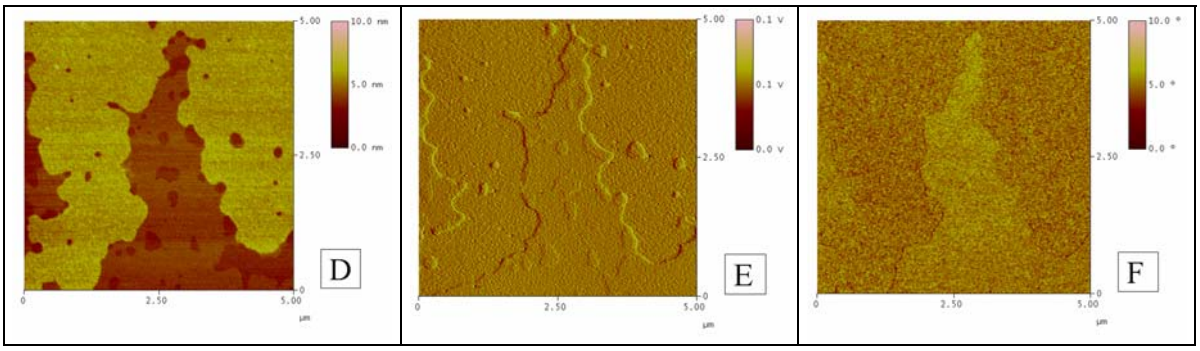

Figure 103. AFM topographic, amplitude and phase images of POPE:CL (0.8:0.2, mol:mol) SPB before (A, B, C) and after (D, E, F) *cyt c* incorporation.

The images in Figure 103 are taken at a higher resolution than the images shown in Figure 94 in section V.3.3. In image A the mica surface, with an *Ra* value of 0.18 nm, cannot be distinguished but three different lipid domains can be seen. The height values are 4.7 nm, 5.10 nm and 6.60 nm above the mica surface and the *Ra* values are 0.14 nm, 0.16 nm and 0.13 nm for the low, intermediate and high lipid domains, respectively. When *cyt c* is injected into the sample (image D) the lipid domains do not change in shape or size. Height and roughness values were then measured from this topographic image. The low and intermediate lipid domains have similar height and *Ra* values to the corresponding measurements before *cyt c* incorporation, but the high lipid domain shows a height of 7.50 nm and a mean *Ra* value of 0.29 nm. These values after *cyt c* injection are higher than for usual lipid bilayers. They are also higher than usual lipid domains, which suggests that some material has been adsorbed onto the domain.

No difference can be seen after *cyt c* injection in the amplitude images (B and E).

In the corresponding phase image before *cyt c* injection (image C) the high lipid domain (yellow structure) can be distinguished from other two lipid domains (red structure), but after *cyt c* injection (image F) the phase contrast between domains in image C shows the opposite gradation. In image F the high lipid domain can be identified as a red structure while the other two lipid domains are identified as yellow structures. Interestingly, the phase contrast between the domains is higher before *cyt c* injection than after the protein is injected. The change in phase contrast could be explained by the fact that *cyt c* is adsorbed only in one of the lipid domains, which creates a surface with the opposite viscolastic properties to those shown before adsorption.

Table XXVII summarizes the topographic parameters of the POPE:CL (0.8:0.2, mol:mol) SPB from Figure 103.

Table XXVII. Parameters of the POPE:CL (0.8:0.2, mol:mol) SPB before and after *cyt c* incorporation.

	Lipid domain	*Cyt c* injection	
		Before	**After**
h (nm)	Low	4.70 ± 0.20	4.80 ± 0.30
	Intermediate	5.10 ± 0.20	5.30 ± 0.30
	High	6.60 ± 0.20	7.50 ± 0.40
***Ra* (nm)**	Low	0.14	0.15
	Intermediate	0.16	0.16
	High	0.13	0.29
	Mica	0.18	0.20

Figure 104 shows a zoomed image of the region highlighted by a white square of the composition from image D in Figure 103.

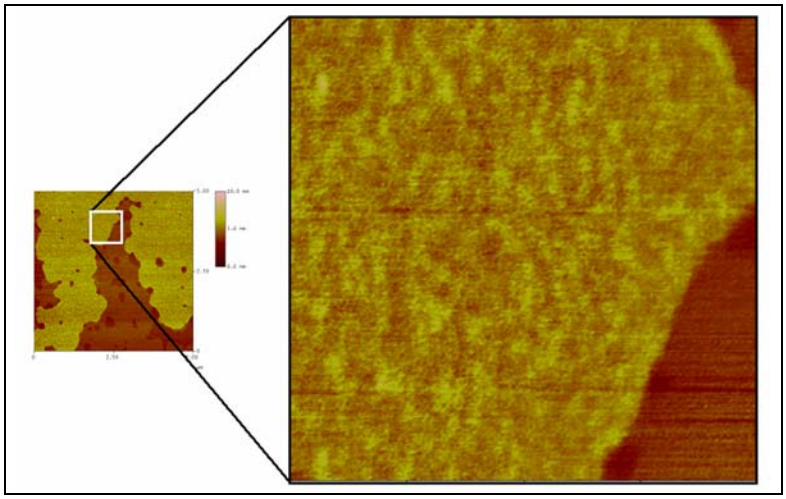

Figure 104. Zoomed topographic AFM image of the high lipid domain after *cyt c* injection into the sample.

The magnified image reveals round and cylindrical structures on the surface of the high lipid domain with a mean width of ~ 20 nm and mean height of ~ 1 nm. These structures have the size of individual proteins when considering the tip convolution effect.

Figure 105 shows an SPB of the same composition in which two lipid domains can be easily distinguished before *cyt c* injection by differences in the colour scale of the topography image (images A and C). The mica surface is clearly visible as a dark red region. This SPB has similar physical parameters to the SPB shown in Figure 94.

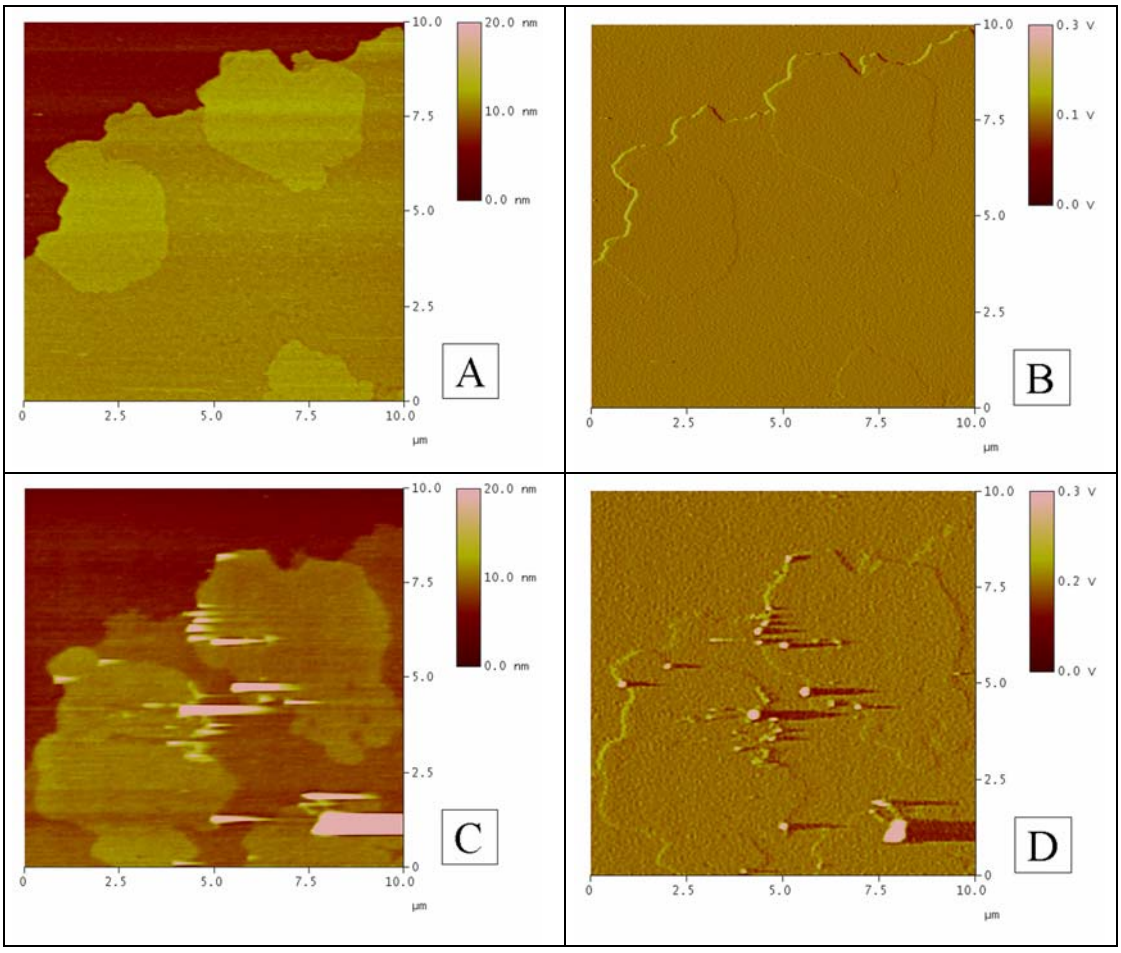

Figure 105. AFM topographic (A and B) and amplitude (C and D) images of a POPE:CL (0.8:0.2, mol:mol) SPB, A) before (images A and B) and B) after (images C and D) *cyt c* injection.

When *cyt c* is injected, small, bright spots with larger height values emerged predominantly at the edges of the upper domain (image 105C). To improve the visualization, the corresponding amplitude image (image 105D) is also shown, in which poorly defined structures, presumably protein aggregates (~ 100 nm diameter), can be observed in the upper domain. In this case, *cyt c* is adsorbed as large aggregates and no individual proteins can be seen in the images.

V.5.4. SPB of POPE:POPC:CL (0.5:0.3:0.2, mol:mol:mol)

Figure 106 shows two sequences of topographic and phase AFM images before (A and B) and after (C and D) *cyt c* incorporation into the sample through the AFM liquid cell.

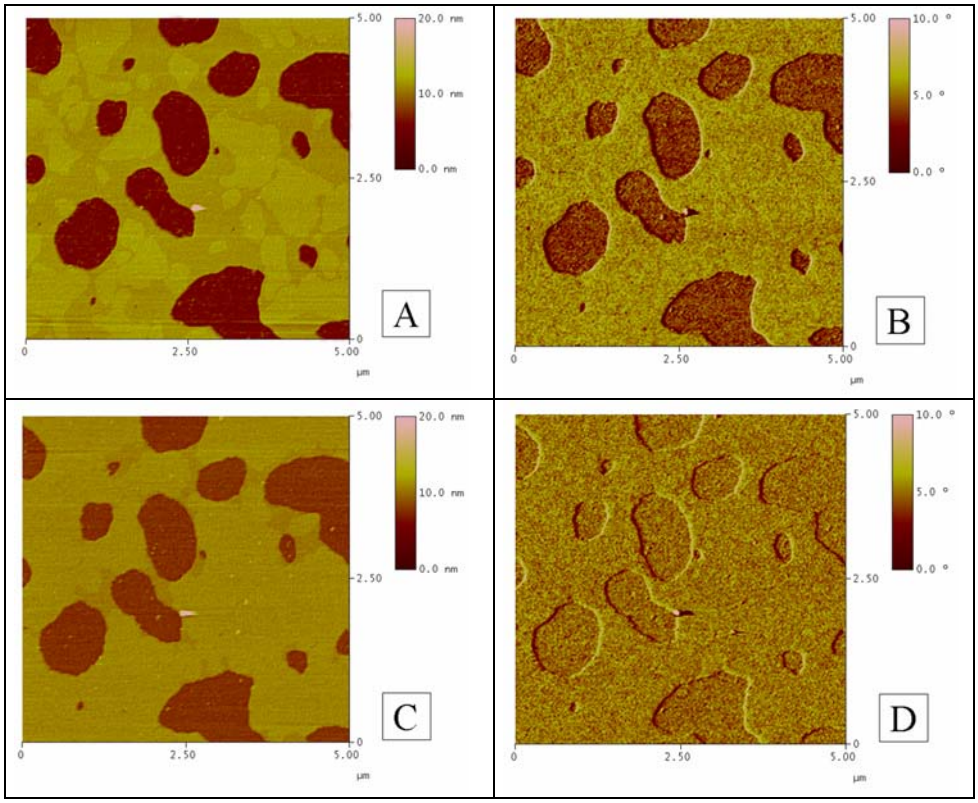

Figure 106. AFM topographic and phase images of a POPE:POPC:CL (0.5:0.3:0.2, mol:mol:mol) SPB before (A and B) and after (C and D) *cyt c* incorporation.

Image A is a topographic image of the SPB in which three different regions can be distinguished. The darkest region is the mica surface with a mean *Ra* value of 0.25 nm and the SPB shows two different lipid domains. The low domain in the image has a mean height of 3.50 nm and an *Ra* value of 0.15 nm, while the high domain is 0.60 nm higher and has a similar *Ra* value. When *cyt c* is injected into the sample (image C) the high lipid domain in image A disappears and a new lipid domain appears. In this image the high lipid domain has a step height of 3.80 nm with an *Ra* value of 0.30 nm, the new lipid domain has a height of 3.10 nm and an identical *Ra* value, while the mica surface has a mean *Ra* value of 0.35 nm. Interestingly, in this image round structures with diameters of ~ 50 nm can be seen. The appearance and disappearance of lipid domains on the SPB surface after *cyt c* injection could be caused by the different temperature of

the injected liquid, which can locally modify the temperature of the sample. This variation in temperature can produce changes in the SPB topography.

The phase image before *cyt c* incorporation (image B) shows the mica surface as dark red region while the SPB surface can be identified as the flat yellow structure. If the SPB surface is analyzed, two lipid domains can be identified as regions with blurred edges. After *cyt c* injection into the sample (image D) the phase contrast between the mica surface and the SPB surface decreases substantially. This could be due to the adsorption of proteins on either the mica or SPB surface, which would modify the viscoelastic properties and becoming more similar than the other. The small protrusions visible in image C after *cyt c* incorporation do not show a different phase contrast to the SPB surface, which suggests that they have similar properties to the SPB surface.

Table XXVIII summarizes the topographic parameters of the POPE:POPC:CL (0.5:0.3:0.2, mol:mol:mol) SPB from Figure 106.

Table XXVIII. Parameters of the POPE:POPC:CL (0.5:0.3:0.2, mol:mol:mol) SPB before and after *cyt c* incorporation.

	Lipid domain	***Cyt c* injection**	
		Before	**After**
h (nm)	Low	-	3.10 ± 0.30
	Intermediate	3.50 ± 0.20	3.80 ± 0.30
	High	4.10 ± 0.30	-
***Ra* (nm)**	Low	-	0.30
	Intermediate	0.15	0.30
	High	0.13	-
	Mica	0.25	0.35